Journal Pre-proofs

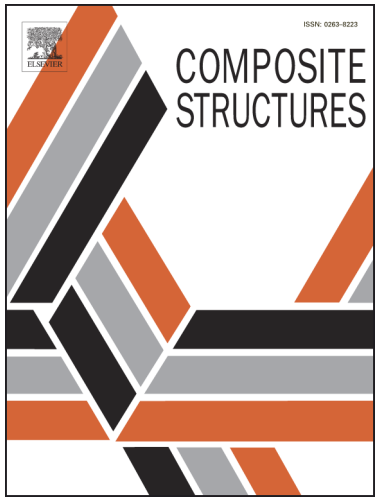

Analysis of stress concentration phenomenon of cylinder laminated shells using higher-order shear deformation Quasi-3D theory

Tran Ngoc Doan, Do Van Thom, Nguyen Truong Thanh, Phan Van Chuong, Nguyen Chi Tho, Nguyen Tri Ta, Hoang Nam Nguyen

PII: S0263-8223(19)33089-2
DOI: https://doi.org/10.1016/j.compstruct.2019.111526
Reference: COST 111526

To appear in: *Composite Structures*

Received Date: 16 August 2019
Revised Date: 27 September 2019
Accepted Date: 4 October 2019

Please cite this article as: Doan, T.N., Van Thom, D., Thanh, N.T., Van Chuong, P., Tho, N.C., Ta, N.T., Nguyen, H.N., Analysis of stress concentration phenomenon of cylinder laminated shells using higher-order shear deformation Quasi-3D theory, *Composite Structures* (2019), doi: https://doi.org/10.1016/j.compstruct.2019.111526

This is a PDF file of an article that has undergone enhancements after acceptance, such as the addition of a cover page and metadata, and formatting for readability, but it is not yet the definitive version of record. This version will undergo additional copyediting, typesetting and review before it is published in its final form, but we are providing this version to give early visibility of the article. Please note that, during the production process, errors may be discovered which could affect the content, and all legal disclaimers that apply to the journal pertain.

© 2019 Published by Elsevier Ltd.

Journal Pre-proofs

Analysis of stress concentration phenomenon of cylinder laminated shells using higher-order shear deformation Quasi-3D theory

Tran Ngoc Doan[1], Do Van Thom[2*], Nguyen Truong Thanh[3], Phan Van Chuong[3], Nguyen Chi Tho[4*], Nguyen Tri Ta[4*], Hoang Nam Nguyen[5]

[1]*Falcuty of Aerospace Engineering, Le Quy Don Technical University, Hanoi City, Vietnam*
[2]*Falcuty of Mechanical Engineering, Le Quy Don Technical University, Hanoi City, Vietnam*
[3]*Institute of Military Science and Technology, Hanoi City, Vietnam*
[4]*Institute of Techniques for Special Engineering, Le Quy Don Technical University, Hanoi City, Vietnam*
[5]*Modeling Evolutionary Algorithms Simulation and Artificial Intelligence, Faculty of Electrical & Electronics Engineering, Ton Duc Thang University, Ho Chi Minh City, Vietnam*

*Corresponding author

Email: thom.dovan.mta@gmail.com (D.V.T); chitho.mta@gmail.com (N.C.T); nguyentrita@gmail.com (N.T.T).

Abstract

This paper presents the stress concentration phenomenon at the points with force jumping, structural jumping and sudden changes of boundary conditions of cylinder laminated shells. The three-dimensional linear elastic equation is transformed into the two-dimensional linear elastic equation of the cylinder laminated shell by using the variational method and analyzing the displacement field into a polynomial function sequence according to the shell thickness. Equilibrium equations are achieved corresponding to the case of analyzing the displacement field into the cubic function. Based on established equations, we study the jumping zone phenomenon of the stress field in the structure. Effects of boundary conditions, the relative thickness and the relative length of the shell are investigated. Then, the application areas of each case based on the computed results are figured out when using these types of structures in engineering practice.

Keywords: Stress concentration, structural jumping, force jumping, variational method, cylindrical laminated shells.

Journal Pre-proofs

1. Introduction

Thin shell structures are used widely in engineering applications such as automotive engineering, aerospace, submarine, nuclear plant, etc., due to their many advantages like high-strength, light-weight, high-impact strength, durable and so on. One of the well-known types is the laminated composite shell. Nowadays, because of the development of science and technology, the durability and rigidity of composite materials are much higher than those of metals, therefore, they account for a large proportion of actual applications. For example, in the aerospace industry, 50 percent of the details of a commercial aircraft are made from composite materials, and the using of these new type materials in order to manufacture the main body and the wings of Boeing 787 can reduce up to 20 percent of its total weigh when comparing with employing aluminum alloys [1]. Besides, when we control the proposition of each component in composite materials, then, the manufacturers can easily customize the mechanical properties of composites according to the working conditions of structures. For instance, for multi-layer composites, based on the response of each layer when changing some parameters such as material and geometrical properties, angle ply, thickness, etc., designers can adjust the properties of each material layer so that they match the particular requirements.

For thin plate and shell structure analyses, based on the assumptions of Kirchhoff–Love, numerous scientists developed linear two-dimensional (2D) plate and shell theories such as Timoshenko and Woinowsky-Krieger [2], Flügge [3], Gol'denveizer [4], Novozhilov [5], Leissa [6] and so on. The mentioned theories are different types of classical deformation theory (CDT). In general, classical deformation theories for plate and shell structures are not suitable when analyzing the mechanical behaviors of thick plate and shell structures. To overcome the disadvantages of these classical theories, Reissner proposed the first-order shear deformation theory (FSDT) [7]. Then, based on FSDT, Kraus [8] and Gould [9] expanded the researches for

Journal Pre-proofs

elastic homogeneous plates and shells. However, similar to CDT, using FSDT requires a shear correction factor to take higher accuracy. As a result, higher-order shear deformation theory (HSDT) has overcome the disadvantages of CDT and FSDT by using the nonlinear polynomial function to describe the shear stress distribution. Reddy [10] used third-order shear deformation theory to analyze mechanical responses of plate and shell structures. However, note that the assumptions proposed by Reddy are not satisfied boundary conditions at the top and bottom surfaces of the structure. Hence, in this work, it is necessary to carry out the process of redefining stress and deformation fields.

In recent years, the number of studies on the third-order shear deformation theory for laminated composite plate and shell structures has been published more and more. Many researchers have introduced the results of the studies on laminated composite plates and shells using the first and higher-order shear deformation theories [11-17]. Hoang Nam Nguyen et al [18] proposed a refined simple first-order shear deformation theory to investigate the static bending and free vibration of functionally graded materials (FGM) plate. The Navier method was applied to improve the cost of calculation time. Also, Hoang Nam Nguyen and colleagues [19] introduced the finite element modelling of a composite shell with shear connectors. In their work, they just used the first-order shear deformation Mindlin plate theory and finite element method (FEM) to establish the equation of motion of the mechanical system subjected to dynamic loads. Then, Hoang Nam Nguyen [20] developed an efficient beam element based on Quasi-3D theory for static bending analysis of functionally graded beams. Nam Vu Hoai and his co-workers [21] firstly used finite element method and phase-field model to carry out the buckling analysis of stiffened functionally graded (FG) plate with cracks. The finite formulation of the plate was derived by employing the first order shear deformation theory (FSDT). In the

recent time, Pham Tien Dat at el. [22] published a work dealt with free vibration analysis of functionally graded shells using an edge-based smoothed finite element method (ES-FEM) combined with the mixed interpolation of tensorial components technique for triangular shell element (MITC3), named ES-MITC3.

However, in their studies, the stress concentration phenomenon has not mentioned much. To deal with this problem, we can list some works as follows. In [23], Lei Jiang et al. studied experimentally and numerically stress concentration factors for tiredness design purposes of the novel tubular joint of concrete-filled square hollow section chord welded to a brace. Yamamoto and colleagues [24] predicted the tensile strengths of unidirectional carbon fiber-reinforced plastic by using a spring element model that considers the surface stress concentration on fibers due to a fracture location in an adjacent fiber. They evaluated the surface stress concentration on the fibers by performing multi-fiber fragmentation tests combining with a spring element model simulation. Based on the obtained results, effects of matrix polymer properties on the surface stress concentration of the fibers were carried out. Özaslan and his co-workers [25] used finite element method to investigate the stress concentration factor for all specimen configurations of unidirectional carbon/epoxy composite specimens with central circular holes. The composite models with different width-to-diameter ratios were tested to investigate the effect of hole size on the stress concentration and strength of the structure. Then, Ahmed et al. [26] employed the traditional experimental and analytical methods to examine the pre damaged stress concentration factor for a composite laminate member with a central circular hole subjected to tensile loading. Next, to extend more comprehensively this important issue, we then have some remarkable works as follows. Fukada [27] presented the phenomenon that significantly affects the stress distribution in damaged laminate composite plates, in which he took into account the ply-to-ply

Journal Pre-proofs

interactions under non-uniform laminate stress fields induce interlaminar and in-plane stresses that are neglected in classical laminate theory. Ehsan Arshid and Ahmad Reza Khorshidvand [28] used Hamilton's variational principle and the classical plate theory (CPT) to derive the governing motion equations for a circular plate made up of a porous material integrated by piezoelectric actuator patches. Then, the free vibration analysis was carried out in order to evaluate the effect of some geometrical and material properties such as thickness ratio, porosity, piezoelectric actuators, variation of piezoelectric actuators-to-porous plate thickness ratio, pores distribution and pores compressibility on the natural vibration, radial and circumferential stresses of mechanical systems. Li [29] employed the extended finite element method (XFEM), layerwise theory (LWT), and develops an extended layerwise method (XLWM) to investigate the accurate description of the multiple delaminations and transverse cracks in double-curved laminated composite shells. Besides, he also used the level set method (LSM) to track the interfaces resulted from the transverse cracks. For the structures deal with elastic foundations, Bekir and Omer [30] carried out geometrically nonlinear free vibration analysis of thin laminated plates resting on non-linear elastic foundations, where they used Winkler-Pasternak type foundation model to describe the elastic foundation of the system. Then, governing equations of motions were derived using the von Karman type nonlinear theory. Omer and Mustafa [31] also presented the bending analysis of Mindlin plates on two-parameter elastic foundations for the first time. In [32], Omer presented linear vibration analysis of isotropic conical shells by discrete singular convolution (DSC). Then, he introduced a discrete singular convolution free vibration analysis of conical panels [33]. In his work, effects of boundary conditions, vertex and subtended angle on the frequencies of conical panel are numerically examined. Most recently, Patni et al. [34] proposed Variable Angle Tow (VAT) composites, which offered increased freedom for tailoring

Journal Pre-proofs

material properties compared to traditional straight-fibre composites. They employed a modelling method that builds upon the recently developed, hierarchical Serendipity Lagrange finite elements. Three-dimensional (3D) stress distribution was obtained using that modelling approach and verified against 3D finite element solutions. The highlight advantage of this approach was the ability to predict effectively accurate 3D stress fields with the minimum cost of calculation time.

In this work, we use the theoretical model of higher order shear deformation theory when taking into account the effect of shear strain and horizontal normal stress [35] to investigate the jumping zone phenomenon when of cylinder laminated shells. The displacement field, in this case, satisfied the energy compatibility conditions proposed by Vasilev and Lurie [36]. Lagrange variational principle is employed to derive the equilibrium equations with the corresponding boundary conditions. The Laplace transform is used to analyze the stress field of cross-ply laminated composite cylindrical shells. The horizontal normal stress component is defined based on the equations of three-dimensional (3D) elasticity theory. Consequently, the displacement, strain, and stress fields are determined completely, then, computed results meet a very good agreement according to 3D elasticity theory.

The structure of this paper is divided into five main sections. The governing equations are given in section 2. Section 3 introduces the characteristic equation and analysis of root forms. Numerical analysis and discussions are presented in section 4. Section 5 concludes some highlight results of this work.

2. The governing equations

2.1. The displacement model

Journal Pre-proofs

Consider a laminated composite cylindrical shell in the orthogonal curvilinear coordinate systems $O\xi\theta z$. The structure includes n layers, the total thickness h, each layer is a homogeneous fiber-reinforced composite material with the geometrical parameters as shown in Figure 1. The neutral plane coincides with the middle plane of the shell. The distances from the neutral plane to the top surface and the bottom surface of layer k are h_{k-1} and h_k, respectively. The main direction of fiber reinforcement of each layer coincides with the direction of the local coordinate system $O123$, correspondingly. The angle between the direction of fiber reinforcement and the vertical axis $O\xi$ of the general coordinate system is β.

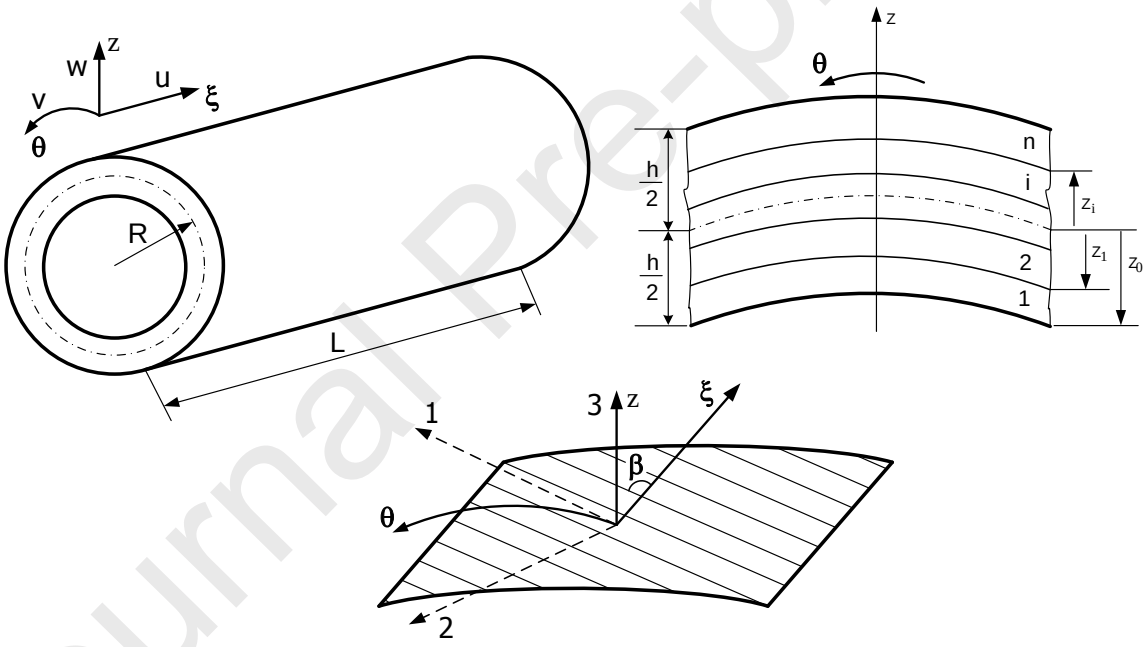

Figure 1. The model of a laminated composite cylindrical shell and its coordinate systems

The displacement field of the shell in the orthogonal curvilinear coordinate systems $O\xi\theta z$ is analyzed as follows

$$u(\xi,\theta,z)=\sum_{k=0}^{K}u_k(\xi,\theta)\frac{z^k}{k!},\ v(\xi,\theta,z)=\sum_{k=0}^{K}v_k(\xi,\theta)\frac{z^k}{k!},\ w(\xi,\theta,z)=\sum_{k=0}^{K-1}w_k(\xi,\theta)\frac{z^k}{k!} \tag{1}$$

Journal Pre-proofs

where $u(\xi,\theta,z)$, $v(\xi,\theta,z)$ and $w(\xi,\theta,z)$ are 3D displacement components of the point $P(\xi,\theta,z)$ at the distance z from the neutral plane ($z = 0$) according to the coordinate axes. u_0, v_0 and w_0 are 2D displacement components of the point $P(\xi,\theta,0)$ according to the coordinate axes. u_1 and v_1 are transverse normal rotations corresponding to the ξ, θ axes. The other displacement components in the equation (1) are the 2D high-order displacements in the analysis according to Taylor series.

2.2. The strain and stress fields

The linear relation between the strain and stress fields of the laminated composite cylindrical shell in the orthogonal curvilinear coordinate systems $O\xi\theta z$ is defined as follows [6]

$$\begin{aligned}&\varepsilon_\xi = \frac{1}{R}\frac{\partial u}{\partial \xi},\ \varepsilon_\theta = \frac{1}{R+z}\left(\frac{\partial v}{\partial \theta}+w\right),\ \gamma_{\xi\theta} = \frac{1}{R}\frac{\partial v}{\partial \xi}+\frac{1}{R+z}\frac{\partial u}{\partial \theta},\\ &\gamma_{\theta z} = \frac{1}{R+z}\frac{\partial w}{\partial \theta}+\frac{\partial v}{\partial z}-\frac{v}{R+z},\ \gamma_{\xi z} = \frac{1}{R}\frac{\partial w}{\partial \xi}+\frac{\partial u}{\partial z},\ \varepsilon_z = \frac{1}{R}\frac{\partial w}{\partial z}\end{aligned} \tag{2}$$

Substituting the expression of displacement components from equation (1) into equation (2), we obtain the expression of strain field as follows

- For the displacement model $K = 3$

$$\begin{aligned}&\varepsilon_\xi = \frac{1}{R}\left(\varepsilon_\xi^0+\chi_\xi z+\varepsilon_\xi^* \frac{z^2}{2}+\chi_\xi^* \frac{z^3}{3!}\right),\ \varepsilon_\theta = \frac{1}{R+z}\left(\varepsilon_\theta^0+\chi_\theta z+\varepsilon_\theta^* \frac{z^2}{2}+\chi_\theta^* \frac{z^3}{3!}\right),\\ &\gamma_{\xi\theta} = \frac{1}{R}\left(\gamma_{\xi\theta}^0+\chi_{\xi\theta} z+\gamma_{\xi\theta}^* \frac{z^2}{2}+\chi_{\xi\theta}^* \frac{z^3}{3!}\right)+\frac{1}{R+z}\left(\lambda_{\xi\theta}^0+\kappa_{\xi\theta} z+\lambda_{\xi\theta}^* \frac{z^2}{2}+\kappa_{\xi\theta}^* \frac{z^3}{3!}\right),\\ &\gamma_{\xi z} = \frac{1}{R}\left(\gamma_{\xi z}^0+\chi_{\xi z} z+\gamma_{\xi z}^* \frac{z^2}{2}+\chi_{\xi z}^* \frac{z^3}{3!}\right),\ \varepsilon_z = \frac{1}{R}\left(\varepsilon_z^0+\chi_z z\right),\\ &\gamma_{\theta z} = \frac{1}{R+z}\left(\gamma_{\theta z}^0+\chi_{\theta z} z+\gamma_{\theta z}^* \frac{z^2}{2}+\chi_{\theta z}^* \frac{z^3}{3!}\right)\end{aligned} \tag{3}$$

- For the displacement model $K = 2$

Journal Pre-proofs

$$\varepsilon_{\xi}=\frac{1}{R}\left(\varepsilon_{\xi}^{0}+\chi_{\xi}z+\varepsilon_{\xi}^{*}\frac{z^{2}}{2}\right),\ \varepsilon_{\theta}=\frac{1}{R+z}\left(\varepsilon_{\theta}^{0}+\chi_{\theta}z+\varepsilon_{\theta}^{*}\frac{z^{2}}{2}\right),\ \varepsilon_{z}=\frac{1}{R}\varepsilon_{z}^{0},$$

$$\gamma_{\xi\theta}=\frac{1}{R}\left(\gamma_{\xi\theta}^{0}+\chi_{\xi\theta}z+\gamma_{\xi\theta}^{*}\frac{z^{2}}{2}\right)+\frac{1}{R+z}\left(\lambda_{\xi\theta}^{0}+\kappa_{\xi\theta}z+\lambda_{\xi\theta}^{*}\frac{z^{2}}{2}\right), \tag{4}$$

$$\gamma_{\xi z}=\frac{1}{R}\left(\gamma_{\xi z}^{0}+\chi_{\xi z}z+\gamma_{\xi z}^{*}\frac{z^{2}}{2}\right),\ \gamma_{\theta z}=\frac{1}{R+z}\left(\gamma_{\theta z}^{0}+\chi_{\theta z}z+\gamma_{\theta z}^{*}\frac{z^{2}}{2}\right)$$

In the above equations, we use some of the following symbols

$$\varepsilon_{\xi}^{0}=\frac{\partial u_{0}}{\partial\xi},\ \chi_{\xi}=\frac{\partial u_{1}}{\partial\xi},\ \varepsilon_{\xi}^{*}=\frac{\partial u_{2}}{\partial\xi},\ \chi_{\xi}^{*}=\frac{\partial u_{3}}{\partial\xi},\ \varepsilon_{z}^{0}=w_{1},\ \chi_{z}=w_{2},$$

$$\varepsilon_{\theta}^{0}=\frac{\partial v_{0}}{\partial\theta}+w_{0},\ \chi_{\theta}=\frac{\partial v_{1}}{\partial\theta}+w_{1},\ \varepsilon_{\theta}^{*}=\frac{\partial v_{2}}{\partial\theta}+w_{2},\ \chi_{\theta}^{*}=\frac{\partial v_{3}}{\partial\theta},$$

$$\gamma_{\xi\theta}^{0}=\frac{\partial v_{0}}{\partial\xi},\ \chi_{\xi\theta}=\frac{\partial v_{1}}{\partial\xi},\ \gamma_{\xi\theta}^{*}=\frac{\partial v_{2}}{\partial\xi},\ \chi_{\xi\theta}^{*}=\frac{\partial v_{3}}{\partial\xi}, \tag{5}$$

$$\lambda_{\xi\theta}^{0}=\frac{\partial u_{0}}{\partial\theta},\ \kappa_{\xi\theta}=\frac{\partial u_{1}}{\partial\theta},\ \lambda_{\xi\theta}^{*}=\frac{\partial u_{2}}{\partial\theta},\ \kappa_{\xi\theta}^{*}=\frac{\partial u_{3}}{\partial\theta},$$

$$\gamma_{\xi z}^{0}=\frac{\partial w_{0}}{\partial\xi}+Ru_{1},\ \chi_{\xi z}=\frac{\partial w_{1}}{\partial\xi}+Ru_{2},\ \gamma_{\xi z}^{*}=\frac{\partial w_{2}}{\partial\xi}+Ru_{3},\ \chi_{\xi z}^{*}=0,$$

$$\gamma_{\theta z}^{0}=\frac{\partial w_{0}}{\partial\theta}+Rv_{1}-v_{0},\ \chi_{\theta z}=\frac{\partial w_{1}}{\partial\theta}+Rv_{2},\ \gamma_{\theta z}^{*}=\frac{\partial w_{2}}{\partial\theta}+Rv_{3}+v_{2},\ \chi_{\theta z}^{*}=2v_{3}$$

The Hooke's law equation for layer *k* in the local coordinate system is expressed as

$$\begin{Bmatrix}\sigma_{1}^{(k)}\\ \sigma_{2}^{(k)}\\ \sigma_{3}^{(k)}\\ \tau_{12}^{(k)}\\ \tau_{13}^{(k)}\\ \tau_{23}^{(k)}\end{Bmatrix}^{L}=\begin{bmatrix}C_{11}^{(k)} & C_{12}^{(k)} & C_{13}^{(k)} & 0 & 0 & 0\\ C_{12}^{(k)} & C_{22}^{(k)} & C_{23}^{(k)} & 0 & 0 & 0\\ C_{13}^{(k)} & C_{23}^{(k)} & C_{33}^{(k)} & 0 & 0 & 0\\ 0 & 0 & 0 & C_{44}^{(k)} & 0 & 0\\ 0 & 0 & 0 & 0 & C_{55}^{(k)} & 0\\ 0 & 0 & 0 & 0 & 0 & C_{66}^{(k)}\end{bmatrix}^{L}.\begin{Bmatrix}\varepsilon_{1}^{(k)}\\ \varepsilon_{2}^{(k)}\\ \varepsilon_{3}^{(k)}\\ \gamma_{12}^{(k)}\\ \gamma_{13}^{(k)}\\ \gamma_{23}^{(k)}\end{Bmatrix}^{L}, \tag{6}$$

The value of each element in the stiffness matrix $\left[C^{(k)}\right]$ can be found in the Appendix.

Equation (6) is re-written in the short form as follow

Journal Pre-proofs

$$\left\{\sigma^{(k)}\right\}=\left[C^{(k)}\right]\left\{\varepsilon^{(k)}\right\} \tag{7}$$

Equation (7) is the relationship between the stress field and the strain field of layer *k* in the local coordinate system $O123$. Because of the local coordinate system $O123$ does not coincide with the general coordinate system $O\xi\theta z$ (see Figure 1), so we need to perform the coordinate transfer for equation (7). Then, the relationship between the stress field and the strain field of layer *k* in the general coordinate system now becomes

$$\left\{\sigma\right\}=\left[T^{(k)}\right]^{t}\left[C^{(k)}\right]\left[T^{(k)}\right]\left\{\varepsilon\right\} \tag{8}$$

in which, $\left\{\sigma\right\}=\left\{\sigma_{\xi}\ \sigma_{\theta}\ \sigma_{z}\ \tau_{\xi\theta}\ \tau_{\xi z}\ \tau_{\theta z}\right\}^{t}$ is the stress vector in the general coordinate system; $\left\{\varepsilon\right\}=\left\{\varepsilon_{\xi}\ \varepsilon_{\theta}\ \varepsilon_{z}\ \gamma_{\xi\theta}\ \gamma_{\xi z}\ \gamma_{\theta z}\right\}^{t}$ is the strain vector in the general coordinate system, the transformation matrix $\left[T^{(k)}\right]$ of the layer k is defined as follow

$$\left[T^{(k)}\right]=\begin{bmatrix}\cos^{2}\beta^{(k)} & \sin^{2}\beta^{(k)} & 0 & 0 & 0 & \sin\beta^{(k)}\cos\beta^{(k)}\\ \sin^{2}\beta^{(k)} & \cos^{2}\beta^{(k)} & 0 & 0 & 0 & -\sin\beta^{(k)}\cos\beta^{(k)}\\ 0 & 0 & 1 & 0 & 0 & 0\\ 0 & 0 & 0 & \cos\beta^{(k)} & -\sin\beta^{(k)} & 0\\ 0 & 0 & 0 & \sin\beta^{(k)} & \cos\beta^{(k)} & 0\\ -\sin 2\beta^{(k)} & \sin 2\beta^{(k)} & 0 & 0 & 0 & \cos^{2}\beta^{(k)}-\sin^{2}\beta^{(k)}\end{bmatrix}.$$

Equation (8) can be re-written as follow

$$\begin{Bmatrix}\sigma_{\xi}\\ \sigma_{\theta}\\ \sigma_{z}\\ \tau_{\xi\theta}\\ \tau_{\xi z}\\ \tau_{\theta z}\end{Bmatrix}=\begin{bmatrix}Q_{11} & Q_{12} & Q_{13} & Q_{14} & 0 & 0\\ Q_{21} & Q_{22} & Q_{23} & Q_{24} & 0 & 0\\ Q_{31} & Q_{32} & Q_{33} & Q_{34} & 0 & 0\\ Q_{41} & Q_{42} & Q_{43} & Q_{44} & 0 & 0\\ 0 & 0 & 0 & 0 & Q_{55} & Q_{56}\\ 0 & 0 & 0 & 0 & Q_{65} & Q_{66}\end{bmatrix}\begin{Bmatrix}\varepsilon_{\xi}\\ \varepsilon_{\theta}\\ \varepsilon_{z}\\ \gamma_{\xi\theta}\\ \gamma_{\xi z}\\ \gamma_{\theta z}\end{Bmatrix}. \tag{9}$$

The value of each element in the general stiffness matrix $\left[Q\right]$ can be found in Appendix.

Journal Pre-proofs

2.3. Equilibrium equations and boundary conditions

To establish the equilibrium equation we use the Lagrange variational principle, the total potential energy must be the minimum value, it means

$$\delta\Pi = \delta\left(U - A\right) = 0 \tag{10}$$

where U is the elastic potential energy, A is the work done by external forces. The variation of the elastic potential energy is defined in the following formula

$$\delta U = \sum_{k=1}^{NL} \int_{\xi} \int_{\theta} \int_{z} \left(\sigma_{\xi} \delta\varepsilon_{\xi} + \sigma_{\theta} \delta\varepsilon_{\theta} + \sigma_{z} \delta\varepsilon_{z} + \tau_{\xi\theta} \delta\gamma_{\xi\theta} + \tau_{\xi z} \delta\gamma_{\xi z} + \tau_{\theta z} \delta\gamma_{\theta z} \right) R^2 \left(1 + \frac{z}{R} \right) d\xi d\theta dz$$

We assume that the shell structure is impacted by the radial distributed load q^{+} on the outer surface and the radial distributed load q^{-} on the inner surface.

$$\delta A = \int_{\xi} \int_{\theta} \left[q^{+} \delta w^{+} \left(1 + \frac{h}{2R} \right) + q^{-} \delta w^{-} \left(1 - \frac{h}{2R} \right) \right] R^2 d\xi d\theta$$

in which $w^{+} = w_0 + \frac{h}{2} w_1 + \frac{h^2}{8} w_2$, $w^{-} = w_0 - \frac{h}{2} w_1 + \frac{h^2}{8} w_2$.

Equilibrium equations are derived by integrating separately the expression (10) according to displacement components, then taking independently the possible displacement equals zero. From there, we get the following equilibrium equation system for each displacement model as follows

Journal Pre-proofs

$$
\begin{aligned}
&\frac{\partial N_\xi}{\partial \xi}+\frac{\partial N_{\theta\xi}}{\partial \theta}=0, && \frac{\partial N_\theta}{\partial \theta}+\frac{\partial N_{\xi\theta}}{\partial \xi}+Q_\theta=0,\\
&\frac{\partial Q_\xi}{\partial \xi}+\frac{\partial Q_\theta}{\partial \theta}-N_\theta-Rp_0=0, && \frac{\partial M_\xi}{\partial \xi}+\frac{\partial M_{\theta\xi}}{\partial \theta}-RQ_\xi=0,\\
&\frac{\partial M_{\xi\theta}}{\partial \xi}+\frac{\partial M_\theta}{\partial \theta}-RQ_\theta=0, && \frac{\partial S_\xi}{\partial \xi}+\frac{\partial S_\theta}{\partial \theta}-M_\theta-RQ_z-Rp_1=0,\\
&\frac{\partial N^*_\xi}{\partial \xi}+\frac{\partial N^*_{\theta\xi}}{\partial \theta}-RS_\xi=0, && \frac{\partial N^*_{\xi\theta}}{\partial \xi}+\frac{\partial N^*_\theta}{\partial \theta}-RS_\theta-Q^*_\theta=0,\\
&\frac{\partial Q^*_\xi}{\partial \xi}+\frac{\partial Q^*_\theta}{\partial \theta}-N^*_\theta-RS_z-Rp_2=0, && \frac{\partial M^*_\xi}{\partial \xi}+\frac{\partial M^*_{\theta\xi}}{\partial \theta}-RQ^*_\xi=0, \text{ (for the model } K=3)\\
&\frac{\partial M^*_{\xi\theta}}{\partial \xi}+\frac{\partial M^*_\theta}{\partial \theta}-RQ^*_\theta-2S^*_\theta=0 \text{ (for the model } K=3)
\end{aligned}
\tag{11}
$$

In equation (11), we use symbols for the extend internal forces as follows

$$
\begin{aligned}
&\left[N_\xi \;\; M_\xi \;\; N^*_\xi \;\; M^*_\xi\right]=\sum_{k=1}^{n}\int_{h_{(k-1)}}^{h_{(k)}}\sigma^{(k)}_\xi\left(1+\frac{z}{R}\right)\left[1 \;\; z \;\; \frac{z^2}{2} \;\; \frac{z^3}{6}\right]dz,\\
&\left[N_\theta \;\; M_\theta \;\; N^*_\theta \;\; M^*_\theta\right]=\sum_{k=1}^{n}\int_{h_{(k-1)}}^{h_{(k)}}\sigma^{(k)}_\theta\left[1 \;\; z \;\; \frac{z^2}{2} \;\; \frac{z^3}{6}\right]dz,\\
&\left[Q_z \;\; S_z\right]=\sum_{k=1}^{n}\int_{h_{(k-1)}}^{h_{(k)}}\sigma^{(k)}_z\left(1+\frac{z}{R}\right)\left[1 \;\; z\right]dz,\\
&\left[N_{\theta\xi} \;\; M_{\theta\xi} \;\; N^*_{\theta\xi} \;\; M^*_{\theta\xi}\right]=\sum_{k=1}^{n}\int_{h_{(k-1)}}^{h_{(k)}}\tau^{(k)}_{\theta\xi}\left[1 \;\; z \;\; \frac{z^2}{2} \;\; \frac{z^3}{6}\right]dz,\\
&\left[N_{\xi\theta} \;\; M_{\xi\theta} \;\; N^*_{\xi\theta} \;\; M^*_{\xi\theta}\right]=\sum_{k=1}^{n}\int_{h_{(k-1)}}^{h_{(k)}}\tau^{(k)}_{\xi\theta}\left(1+\frac{z}{R}\right)\left[1 \;\; z \;\; \frac{z^2}{2} \;\; \frac{z^3}{6}\right]dz,\\
&\left[Q_\xi \;\; S_\xi \;\; Q^*_\xi\right]=\sum_{k=1}^{n}\int_{h_{(k-1)}}^{h_{(k)}}\tau^{(k)}_{\xi z}\left(1+\frac{z}{R}\right)\left[1 \;\; z \;\; \frac{z^2}{2}\right]dz,\\
&\left[Q_\theta \;\; S_\theta \;\; Q^*_\theta \;\; S^*_\theta\right]=\sum_{k=1}^{n}\int_{h_{(k-1)}}^{h_{(k)}}\tau^{(k)}_{\theta z}\left[1 \;\; z \;\; \frac{z^2}{2} \;\; \frac{z^3}{6}\right]dz,
\end{aligned}
\tag{12}
$$

Journal Pre-proofs

$$p_i = q^+\left(1+\frac{h}{2R}\right)\frac{h^i}{2^i i!}+q^-\left(1-\frac{h}{2R}\right)\frac{(-h)^i}{2^i i!},\ i=0,1,2$$

The boundary condition of equation (11) has the following cases

- For boundary condition $\xi = const$

$$\begin{aligned}
&N_\xi = \overline{N}_\xi \ \vee\ u_0 = \bar{u}_0,\ N_{\xi\theta} = \overline{N}_{\xi\theta} \ \vee\ v_0 = \bar{v}_0,\ Q_\xi = \bar{Q}_\xi \ \vee\ w_0 = \bar{w}_0,\\
&M_\xi = \overline{M}_\xi \ \vee\ u_1 = \bar{u}_1,\ M_{\xi\theta} = \overline{M}_{\xi\theta} \ \vee\ v_1 = \bar{v}_1,\ S_\xi = \bar{S}_\xi \ \vee\ w_1 = \bar{w}_1,\\
&N^*_\xi = \overline{N}^*_\xi \ \vee\ u_2 = \bar{u}_2,\ N^*_{\xi\theta} = \overline{N}^*_{\xi\theta} \ \vee\ v_2 = \bar{v}_2,\ Q^*_\xi = \bar{Q}^*_\xi \ \vee\ w_2 = \bar{w}_2,\\
&M^*_\xi = \overline{M}^*_\xi \ \vee\ u_3 = \bar{u}_3,\ M^*_{\xi\theta} = \overline{M}^*_{\xi\theta} \ \vee\ v_3 = \bar{v}_3,
\end{aligned} \tag{13}$$

- For boundary condition $\theta = const$

$$\begin{aligned}
&N_{\theta\xi} = \overline{N}_{\theta\xi} \ \vee\ u_0 = \bar{u}_0,\ N_\theta = \overline{N}_\theta \ \vee\ v_0 = \bar{v}_0,\ Q_\theta = \bar{Q}_\theta \ \vee\ w_0 = \bar{w}_0,\\
&M_{\theta\xi} = \overline{M}_{\theta\xi} \ \vee\ u_0 = \bar{u}_0,\ M_\theta = \overline{M}_\theta \ \vee\ v_1 = \bar{v}_1,\ S_\theta = \bar{S}_\theta \ \vee\ w_1 = \bar{w}_1,\\
&N^*_{\theta\xi} = \overline{N}^*_{\theta\xi} \ \vee\ u_2 = \bar{u}_2,\ N^*_\theta = \overline{N}^*_\theta \ \vee\ v_2 = \bar{v}_2,\ Q^*_\theta = \bar{Q}^*_\theta \ \vee\ w_2 = \bar{w}_2,\\
&M^*_{\theta\xi} = \overline{M}^*_{\theta\xi} \ \vee\ u_3 = \bar{u}_3,\ M^*_\theta = \overline{M}^*_\theta \ \vee\ v_3 = \bar{v}_3.
\end{aligned} \tag{14}$$

The boundary conditions (13) and (14) cover all types of boundary conditions in the actual calculation and the number of boundary conditions equal to the number of steps of the differential equation system for the displacement field.

In the case of structure is a full cylindrical shell, the boundary condition (14) is replaced by the cyclic boundary condition abided by the θ coordinate. The boundary condition (13) for some common cases in practice is given as follows

- For fully clamped supported boundary

$$u_0 = u_1 = u_2 = u_3 = 0,\ v_0 = v_1 = v_2 = v_3 = 0,\ w_0 = w_1 = w_2 = 0,$$

- For fully free supported boundary

Journal Pre-proofs

$$N_\xi = M_\xi = N_\xi^* = M_\xi^* = 0,\ N_{\xi\theta} = M_{\xi\theta} = N_{\xi\theta}^* = M_{\xi\theta}^* = 0,\ Q_\xi = S_\xi = Q_\xi^* = 0,$$

- For fully simply supported boundary

$$N_\xi = M_\xi = N_\xi^* = M_\xi^* = 0,\ v_0 = v_1 = v_2 = v_3 = 0,\ w_0 = w_1 = w_2 = 0.$$

Equilibrium equation (11) gives us the $3K+2$ differential-difference equation system for $3K+2$ displacement components u_k, v_k, w_k and its degree of freedom is $2(3K+2)$. Solving above equation we obtain the general roots with the internal constants; these constants can be found by using boundary conditions (13) and (14).

Substituting the root expression of the displacement into equations (3), (4) and (5) we get the deformation of the shell structure. To find the stresses σ_ξ, σ_θ and $\tau_{\xi\theta}$, we use the Hooke's principle equation (9) then integrating the equilibrium equation of the 3D elasticity theory.

$$\tau_{\xi z} = -\frac{1}{R+z}\int_{-h/2}^{z}\left[\left(1+\frac{z}{R}\right)\frac{\partial\sigma_\xi}{\partial\xi}+\frac{\partial\tau_{\xi\theta}}{\partial\theta}\right]dz,$$

$$\tau_{\theta z} = -\frac{R}{(R+z)^2}\int_{-h/2}^{z}\left[\left(1+\frac{z}{R}\right)\frac{\partial\sigma_\theta}{\partial\theta}+\left(1+\frac{z}{R}\right)^2\frac{\partial\tau_{\xi\theta}}{\partial\xi}\right]dz,$$

$$\sigma_z = -\frac{1}{R+z}\int_{-h/2}^{z}\left[\left(1+\frac{z}{R}\right)\frac{\partial\tau_{\xi z}}{\partial\xi}+\frac{\partial\tau_{\theta z}}{\partial\theta}-\sigma_\theta\right]dz+\frac{R-h/2}{R+h/2}q^-.$$

3. Characteristic equation and analysis of root forms

For the case the structure is made from cross-ply laminated composite, equation (11) is re-written according to the displacement of the following form

Journal Pre-proofs

$$
\begin{aligned}
&\sum_{i=0}^{K}\left(H_{1i}^{l}+H_{1i,11}^{l}\frac{\partial^2}{\partial\xi^2}+H_{1i,22}^{l}\frac{\partial^2}{\partial\theta^2}\right)u_i+\sum_{i=0}^{K}H_{2i,12}^{l}\frac{\partial^2}{\partial\xi\partial\theta}v_i+\\
&\quad+\sum_{i=0}^{K-1}H_{3i,1}^{l}\frac{\partial}{\partial\xi}w_i=0,\quad l=1,...,(K+1),\\
&\sum_{i=0}^{K}H_{1i,12}^{m}\frac{\partial^2}{\partial\xi\partial\theta}u_i+\sum_{i=0}^{K}\left(H_{2i}^{m}+H_{2i,11}^{m}\frac{\partial^2}{\partial\xi^2}+H_{2i,22}^{m}\frac{\partial^2}{\partial\theta^2}\right)v_i+\\
&\quad+\sum_{i=0}^{K-1}H_{3i,2}^{m}\frac{\partial}{\partial\theta}w_i=0,\quad m=(K+2),...,(2K+2),\\
&\sum_{i=0}^{K}H_{1i,1}^{n}\frac{\partial}{\partial\xi}u_i+\sum_{i=0}^{K-1}\left(H_{3i}^{n}+H_{3i,11}^{n}\frac{\partial^2}{\partial\xi^2}+H_{3i,22}^{n}\frac{\partial^2}{\partial\theta^2}\right)w_i+\\
&\quad+\sum_{i=0}^{K}H_{2i,2}^{n}\frac{\partial}{\partial\theta}v_i=H_{q^+}^{n}q^{+}-H_{q^-}^{n}q^{-},\quad n=(2K+3),...,(3K+2),
\end{aligned}
\tag{15}
$$

herein, the coefficients H are the constants, which depend on the number of layers. R is the radius; h is the relative thickness; Poisson's ratio μ_{ij} and Young's modulus E_{ij} of the entire structure are defined through homogenizing the coefficients of two equations (11) and (15).

In order to satisfy the cyclic boundary condition abided by the θ coordinate, we need to expand the displacement field and the load according to the single trigonometric series as follows

$$
\begin{aligned}
u_i(\xi,\theta)&=U_{i0}(\xi)+\sum_{m=1}^{\infty}\left[U_{im}^{1}(\xi)\cos m\theta+U_{im}^{2}(\xi)\sin m\theta\right],\\
v_i(\xi,\theta)&=V_{i0}(\xi)+\sum_{m=1}^{\infty}\left[V_{im}^{1}(\xi)\sin m\theta-V_{im}^{2}(\xi)\cos m\theta\right],\\
w_j(\xi,\theta)&=W_{j0}(\xi)+\sum_{m=1}^{\infty}\left[W_{jm}^{1}(\xi)\cos m\theta+W_{jm}^{2}(\xi)\sin m\theta\right],\\
q^{\pm}(\xi,\theta)&=Q_{0}^{\pm}(\xi)+\sum_{m=1}^{\infty}\left[Q_{m}^{1\pm}(\xi)\cos m\theta+Q_{m}^{2\pm}(\xi)\sin m\theta\right].
\end{aligned}
\tag{16}
$$

Substituting equation (16) into equation (15) then perform some simple mathematical transformations, we obtain differential equations to determine $U_{i0}(\xi)$, $W_{j0}(\xi)$ functions as follows

Journal Pre-proofs

$$\sum_{i=0}^{K}\left(H_{1i}^{l}+H_{1i,11}^{l}\frac{d^2}{d\xi^2}\right)U_{i0}+\sum_{i=0}^{K-1}H_{3i,1}^{l}\frac{dW_{j0}}{d\xi}=0,\ l=1,...,(K+1),$$
$$\sum_{i=0}^{K}H_{1i,1}^{n}\frac{dU_{i0}}{d\xi}+\sum_{i=0}^{K-1}\left(H_{3i}^{n}+H_{3i,11}^{n}\frac{d^2}{d\xi^2}\right)W_{j0}=H_{q^+}^{n}Q_0^{+}-H_{q^-}^{n}Q_0^{-},\ n=(2K+3),...,(3K+2). \quad (17)$$

In the case of the shell is subjected to symmetrical axial load, so the component $V_{i0}(\xi)=0$

For the functions $U_{im}^{1}(\xi)$, $V_{im}^{1}(\xi)$, $W_{jm}^{1}(\xi)$ và $U_{im}^{2}(\xi)$, $V_{im}^{2}(\xi)$ and $W_{jm}^{2}(\xi)$, we obtain the system of differential equations with the same form as follows

$$\begin{aligned}
&\sum_{i=0}^{K}\left(H_{1i}^{l}+H_{1i,11}^{l}\frac{d^2}{d\xi^2}-m^2H_{1i,22}^{l}\right)U_{im}+m\sum_{i=0}^{K}H_{2i,12}^{l}\frac{d}{d\xi}V_{im}+\\
&\quad+\sum_{i=0}^{K-1}H_{3i,1}^{l}\frac{d}{d\xi}W_{im}=0,\quad l=1,...,(K+1),\\
&-m\sum_{i=0}^{K}H_{1i,12}^{m}\frac{d}{d\xi}U_{im}+\sum_{i=0}^{K}\left(H_{2i}^{m}+H_{2i,11}^{m}\frac{d^2}{d\xi^2}-m^2H_{2i,22}^{m}\right)V_{im}-\\
&\quad-m\sum_{i=0}^{K-1}H_{3i,2}^{m}W_{im}=0,\quad m=(K+2),...,(2K+2),\\
&\sum_{i=0}^{K}H_{1i,1}^{n}\frac{d}{d\xi}U_{im}+\sum_{i=0}^{K-1}\left(H_{3i}^{n}+H_{3i,11}^{n}\frac{d^2}{d\xi^2}-m^2H_{3i,22}^{n}\right)W_{im}+\\
&\quad+m\sum_{i=0}^{K}H_{2i,2}^{n}V_{im}=H_{q^+}^{n}Q_m^{+}-H_{q^-}^{n}Q_m^{-},\quad n=(2K+3),...,(3K+2),
\end{aligned} \quad (18)$$

In equation (18) we neglect the superscript indexes 1 and 2 of the quantities U_{im}, V_{im} and W_{im}.

In shell theories, the strain-stress field is divided into the fundamental strain-stress field and the boundary strain-stress field. In addition, the strain-stress field of the shell structure depends on root types of characteristic equation of systems (17) and (18). Therefore, to analyze the strain-stress field, we should study the solutions of the characteristic equation of systems (17) and (18) in some specific cases $K=2, K=3$. The characteristic equation corresponding to each

Journal Pre-proofs

system of differential equations is replaced by differential operator $d/d\xi$ with variation p. Then let the right-hand factor determinant of the corresponding system of equations received equals to 0.

Firstly, we analyze the system of equations (17) as follows

- For the model $K = 2$

The characteristic equation of (17) becomes

$$\Delta_1 = p^2 \sum_{n=0}^{4} (-1)^n K_n^1 p^{2n} = 0 \tag{19}$$

Besides the trivial roots, equation (19) also has the following roots

+ Case 1: A pair of conjugate complexes $\pm p_1 \pm iq_1$ and a pair of real roots $\pm p_2, \pm p_3$ with inequality $p_1 \neq p_2, p_3$. Thus, the general root of (17) is expressed as follow

$$F_1 = \left(a_1 \sin q_1\xi + a_2 \cos q_1\xi\right)e^{p_1\xi} + \left(a_3 \sin q_1\xi + a_4 \cos q_1\xi\right)e^{-p_1\xi} + \\ + a_5 e^{p_2\xi} + a_6 e^{-p_2\xi} + a_7 e^{p_3\xi} + a_8 e^{-p_3\xi}$$

+ Case 2: Two pairs of conjugate complexes $\pm p_1 \pm iq_1$, $\pm p_2 \pm iq_2$ with inequality $p_1 \neq p_2, q_1 \neq q_2$. In this case, the general root of (17) is written as follow

$$F_2 = \left(a_1 \sin q_1\xi + a_2 \cos q_1\xi\right)e^{p_1\xi} + \left(a_3 \sin q_1\xi + a_4 \cos q_1\xi\right)e^{-p_1\xi} + \\ + \left(a_5 \sin q_2\xi + a_6 \cos q_2\xi\right)e^{p_2\xi} + \left(a_7 \sin q_2\xi + a_8 \cos q_2\xi\right)e^{-p_2\xi}$$

- For the model $K = 3$

The characteristic equation of (17) becomes

$$\Delta_2 = p^2 \sum_{n=0}^{6} (-1)^n K_n^2 p^{2n} = 0. \tag{20}$$

Besides the trivial roots, equation (20) also has the following roots

Journal Pre-proofs

+ Case 1: A pair of conjugate complexes $\pm p_1 \pm q_1$ and three pairs of real roots $\pm p_3, \pm p_4, \pm p_5$ with inequality $p_1 \neq p_2, p_3, p_4, p_5$. Herein, the general root of (17) is expressed as follow

$$F_3 = \left(a_1 \sin q_1\xi + a_2 \cos q_1\xi\right)e^{p_1\xi} + \left(a_3 \sin q_1\xi + a_4 \cos q_1\xi\right)e^{-p_1\xi} + a_5 e^{p_2\xi} + a_6 e^{-p_2\xi} + a_7 e^{p_3\xi} + a_8 e^{-p_3\xi} + a_9 e^{p_4\xi} + a_{10} e^{-p_4\xi} + a_{11} e^{p_5\xi} + a_{12} e^{-p_5\xi}$$

+ Case 2: Two pairs of conjugate complexes $\pm p_1 \pm iq_1$, $\pm p_2 \pm iq_2$ and two pairs of real roots $\pm p_3$, $\pm p_4$ with inequality $p_1 \neq p_2, p_3, q_1 \neq q_2$. Thus, the general root of (17) is defined as follow

$$\begin{aligned} F_4 = {} & \left(a_1 \sin q_1\xi + a_2 \cos q_1\xi\right)e^{p_1\xi} + \left(a_3 \sin q_1\xi + a_4 \cos q_1\xi\right)e^{-p_1\xi} + \\ & + \left(a_5 \sin q_2\xi + a_6 \cos q_2\xi\right)e^{p_2\xi} + \left(a_7 \sin q_2\xi + a_8 \cos q_2\xi\right)e^{-p_2\xi} + \\ & + a_9 e^{p_3\xi} + a_{10} e^{-p_3\xi} + a_{11} e^{p_4\xi} + a_{12} e^{-p_4\xi} \end{aligned}$$

Next, we analyze the system of equations (18) as follows

- For the model $K = 2$

The characteristic equation of (18) becomes

$$\Delta_3 = \sum_{n=0}^{8} (-1)^n K_n^3 p^{2n} = 0 \tag{21}$$

Equation (21) has the following roots

+ Case 1: Two pairs of conjugate complexes $\pm p_1 \pm iq_1$, $\pm p_2 \pm iq_2$ and four pairs of real roots $\pm p_3$, $\pm p_4$, $\pm p_5$, $\pm p_6$ with inequality $p_1 \neq p_2, p_3, p_4, p_5, p_6$. Herein, the general root of (18) is expressed as follow

$$\begin{aligned} F_5 = {} & \left(a_1 \sin q_1\xi + a_2 \cos q_1\xi\right)e^{p_1\xi} + \left(a_3 \sin q_1\xi + a_4 \cos q_1\xi\right)e^{-p_1\xi} + \\ & + \left(a_5 \sin q_2\xi + a_6 \cos q_2\xi\right)e^{p_2\xi} + \left(a_7 \sin q_2\xi + a_8 \cos q_2\xi\right)e^{-p_2\xi} + \\ & + a_9 e^{p_3\xi} + a_{10} e^{-p_3\xi} + a_{11} e^{p_4\xi} + a_{12} e^{-p_4\xi} + a_{13} e^{p_5\xi} + a_{14} e^{-p_5\xi} + a_{15} e^{p_6\xi} + a_{16} e^{-p_6\xi} \end{aligned}$$

Journal Pre-proofs

+ Case 2: Three pairs of conjugate complexes $\pm p_1 \pm iq_1$, $\pm p_2 \pm iq_2$, $\pm p_3 \pm iq_3$ and two pairs of real roots $\pm p_4$, $\pm p_5$ with inequality $p_1 \square\ p_2 < p_3, p_4, p_5$. In this case, the general root of (18) is defined as follow

$$\begin{aligned} F_6 = &\left(a_1 \sin q_1\xi + a_2 \cos q_1\xi\right)e^{p_1\xi} + \left(a_3 \sin q_1\xi + a_4 \cos q_1\xi\right)e^{-p_1\xi} + \\ &+ \left(a_5 \sin q_2\xi + a_6 \cos q_2\xi\right)e^{p_2\xi} + \left(a_7 \sin q_2\xi + a_8 \cos q_2\xi\right)e^{-p_2\xi} + \\ &+ \left(a_9 \sin q_3\xi + a_{10} \cos q_3\xi\right)e^{p_3\xi} + \left(a_{11} \sin q_3\xi + a_{12} \cos q_3\xi\right)e^{-p_3\xi} + \\ &+ a_{13}e^{p_4\xi} + a_{14}e^{-p_4\xi} + a_{15}e^{p_5\xi} + a_{16}e^{-p_5\xi} \end{aligned}$$

- For the model $K = 3$

The characteristic equation of (18) becomes

$$\Delta_4 = \sum_{n=0}^{11} (-1)^n K_n^4 p^{2n} = 0 \tag{22}$$

Equation (22) has the following roots

+ Case 1: Three pairs of conjugate complexes $\pm p_1 \pm iq_1$, $\pm p_2 \pm iq_2$, $\pm p_3 \pm iq_3$ and five pairs of real roots $\pm p_4$, $\pm p_5$, $\pm p_6$, $\pm p_7$, $\pm p_8$ with inequality $q_1 \square\ q_2 < q_3$, $p_1 \square\ p_2 < p_3, p_4, p_5, p_6, p_7, p_8$. Herein, the general root of (18) is expressed as follow

$$\begin{aligned} F_7 = &\left(a_1 \sin q_1\xi + a_2 \cos q_1\xi\right)e^{p_1\xi} + \left(a_3 \sin q_1\xi + a_4 \cos q_1\xi\right)e^{-p_1\xi} + \\ &+ \left(a_5 \sin q_2\xi + a_6 \cos q_2\xi\right)e^{p_2\xi} + \left(a_7 \sin q_2\xi + a_8 \cos q_2\xi\right)e^{-p_2\xi} + \\ &+ \left(a_9 \sin q_3\xi + a_{10} \cos q_3\xi\right)e^{p_3\xi} + \left(a_{11} \sin q_3\xi + a_{12} \cos q_3\xi\right)e^{-p_3\xi} + \\ &+ a_{13}e^{p_4\xi} + a_{14}e^{-p_4\xi} + a_{15}e^{p_5\xi} + a_{16}e^{-p_5\xi} + a_{17}e^{p_6\xi} + a_{18}e^{-p_6\xi} + \\ &+ a_{19}e^{p_7\xi} + a_{20}e^{-p_7\xi} + a_{21}e^{p_8\xi} + a_{22}e^{-p_8\xi} \end{aligned}$$

+ Case 2: Four pairs of conjugate complexes $\pm p_1 \pm iq_1$, $\pm p_2 \pm iq_2$, $\pm p_3 \pm iq_3$, $\pm p_4 \pm iq_4$ and three pairs of real roots $\pm p_5$, $\pm p_6$, $\pm p_7$ with inequality $q_1 \square\ q_2 < q_3, q_4$, $p_1 \square\ p_2 < p_3, p_4, p_5, p_6, p_7$. In this case, the general root of (18) is defined as follow

Journal Pre-proofs

$$F_8 = \left(a_1 \sin q_1\xi + a_2 \cos q_1\xi\right)e^{p_1\xi} + \left(a_3 \sin q_1\xi + a_4 \cos q_1\xi\right)e^{-p_1\xi} +$$
$$+\left(a_5 \sin q_2\xi + a_6 \cos q_2\xi\right)e^{p_2\xi} + \left(a_7 \sin q_2\xi + a_8 \cos q_2\xi\right)e^{-p_2\xi} +$$
$$+\left(a_9 \sin q_3\xi + a_{10} \cos q_3\xi\right)e^{p_3\xi} + \left(a_{11} \sin q_3\xi + a_{12} \cos q_3\xi\right)e^{-p_3\xi} +$$
$$+\left(a_{13} \sin q_4\xi + a_{14} \cos q_4\xi\right)e^{p_4\xi} + \left(a_{15} \sin q_4\xi + a_{16} \cos q_4\xi\right)e^{-p_4\xi} +$$
$$+ a_{17}e^{p_5\xi} + a_{18}e^{-p_5\xi} + a_{19}e^{p_6\xi} + a_{20}e^{-p_6\xi} + a_{21}e^{p_7\xi} + a_{22}e^{-p_7\xi}$$

To illustrate the obtained results above, we consider the roots of the characteristic equation for a cylindrical laminated composite shell under symmetrical axial load. The geometric parameters include L/R=4, h=0.1 with the different relative thicknesses.

The computed results of this work are compared with those of Mindlin [37] as listed in Table 1.

Table 1

The roots of the characteristic equation for cylindrical laminated composite shell [0/90°/0]; material properties (Graphite-Epoxy (AS/3501) [10]) E_1=137.9, E_2= E_3=9.0, G_{12}=G_{13}=7.1, G_{23}=6.2, $\nu_{12} = \nu_{13} = 0.3, \nu_{23} = 0.49$

	S	10	20	30	40	50	100
p_1	$K=3$	3.31	4.43	5.33	6.09	6.777	9.46
	$K=2$	3.56	4.83	5.83	6.69	7.45	10.44
	Mindlin [37]	3.61	4.89	5.91	6.70	7.54	10.57
q_1	$K=3$	2.56	3.91	4.90	5.72	6.44	9.23
	$K=2$	2.95	4.42	5.50	6.40	7.19	10.26
	Mindlin [37]	2.98	4.47	5.56	6.47	7.27	10.38
p_2	$K=3$	31.06	62.1	93.19	124.3	155.32	310.65
	$K=2$	31.08	62.1	93.20	124.3	155.33	310.65
q_2	$K=3$	8.12	16.2	24.34	32.5	40.56	81.13
	$K=2$	8.09	16.2	24.33	32.4	40.56	81.12
p_3	$K=3$	12.82	25.7	38.57	51.4	64.29	128.59
p_4	$K=3$	102.34	204.6	306.89	409.2	511.47	1022.93

Journal Pre-proofs

Table 2

The roots of the characteristic equation for cylindrical laminated isotropic shell; material properties [10] $E_2 = E_1/25$, $E_1 = 172.4$, $G_{12} = G_{13} = 0.5E_2$, $G_{23} = 0.2E_2$, $\nu_{12} = \nu_{13} = \nu_{23} = 0.25$.

	S	10	20	30	40	50	100
p_1	$K = 3$	2.07	2.66	3.14	3.56	3.94	5.44
	$K = 2$	2.16	2.85	3.40	3.88	4.30	5.98
	Mindlin [37]	2.21	2.91	3.46	3.95	4.30	6.08
q_1	$K = 3$	1.20	2.06	2.66	3.15	3.57	5.18
	$K = 2$	1.47	2.38	3.02	3.54	4.00	5.77
	Mindlin [37]	1.49	2.41	3.06	3.59	4.06	5.86
p_2	$K = 3$	5.10	10.3	15.5	20.6	25.8	51.6
	$K = 2$	6.93	13.9	20.8	27.7	34.7	69.3
p_3	$K = 3$	6.93	13.9	20.8	27.7	34.7	99.3
	$K = 2$	79.7	159.4	239.1	318.8	398.5	797.0
p_4	$K = 3$	79.7	159.4	239.1	318.8	398.5	797.0
p_5	$K = 3$	178.9	357.8	536.7	715.5	894.4	1788.9

Table 3

The roots of the characteristic equation for cylindrical laminated composite shell [0/90°/0]; material properties [10] $E_1 = 172.4$, $E_2 = E_1/25$, $G_{12} = G_{13} = 0.5E_2$, $G_{23} = 0.2E_2$, $\nu_{12} = \nu_{13} = \nu_{23} = 0.25$.

	S	10	30	50	100	500
p_1	$K = 3$	4.43	6.34	7.83	10.69	23.18
	$K = 2$	4.25	6.25	7.77	10.63	23.12
	Mindlin [37]	4.26	6.28	7.78	10.65	23.19
q_1	$K = 3$	1.44	4.83	6.68	9.87	22.82
	$K = 2$	1.74	4.92	6.73	9.90	22.79
	Mindlin [37]	1.74	4.92	6.74	9.92	22.86
p_2	$K = 3$	15.40	47.13	78.56	157.13	491.15
	$K = 2$	9.84	29.53	49.21	98.42	491.20
p_3	$K = 3$	15.72	47.36	78.56	158.02	789.55

Journal Pre-proofs

	$K=2$	76.90	230.51	384.15	768.28	3894.65
p_4	$K=3$	48.15	144.36	240.59	481.17	2439.63
p_5	$K=3$	129.70	388.70	647.78	1295.51	6575.43

From Tables 1-3 we understand that the roots of the characteristic equation are divided into two groups: small roots and large roots. The small roots represent the fundamental strain-stress field of the shell structure, and the large roots describe the boundary phenomena of the shell structure. These phenomena only exist in the areas with sudden changes in structural parameters and external forces. When moving away from the jumping zone phenomena, they are quickly annihilated.

4. Numerical analysis and discussion

4.1. Verification examples

Let us consider a fully simply supported cylinder laminated composite shell with the relative length L/R = 4, the relative thickness $S = R/h$ can be varied. The thicknesses of each layer are equal; the material properties are [38] $E_1 = 25E_2$, $G_{23} = 0.2E_2$, $G_{13} = G_{12} = 0.5E_2$, Poisson's ratio $\nu_{12} = 0.25$; the shell structure under the sinusoidal distributed load on the inner surface $q_{mn} = Q_0 \sin\frac{m\pi\xi R}{L}\cos n\theta$. The shell structure is fully simply supported at two sides. The following computed results in this section correspond to the model $K = 3$. Non-dimensional deflection and stress are calculated as follows

$$\bar{w} = \frac{10E_1.w}{Q_0 HS^4}, \left(\bar{\sigma}_\xi, \bar{\sigma}_\theta\right) = \frac{1}{Q_0 S^2}\left(\sigma_\xi, \sigma_\theta\right), \bar{\tau}_{\xi z} = \frac{\tau_{\xi z}}{Q_0 S}, \bar{\sigma}_z = \frac{\sigma_z}{\sigma_\theta\left(\xi/2, \theta/2\right)} \tag{22}$$

The non-dimensional deflection results in the middle of the laminated composite shell are compared with those of exact solution of Varadan-Bhaskar [38] are presented in Table 4.

Table 4

Journal Pre-proofs

Non-dimensional deflection $\bar{w}$ at the middle of the laminated composite shell for different relative thicknesses; $L/R=4; S=R/h; m=1; n=4$

S	[90°]		[90°/0]		[90°/0/90°]		$[90°/0/90°/0/90°]_2$	
	Present	V&B [38]	Present	V&B [38]	Present	V&B [38]	Present	V&B [38]
4	2.7723	2.7830	7.3555	6.1000	3.8021	4.0090	3.9979	4.2060
10	0.9172	0.9189	3.6490	3.3300	1.0971	1.2230	1.3437	1.3800
50	0.5384	0.5385	2.2516	2.2420	0.5436	0.5495	0.7609	0.7622
100	0.5169	0.5170	1.3682	1.3670	0.4703	0.4715	0.6259	0.6261
500	0.3060	0.3060	0.1005	0.1005	0.1027	0.1027	0.1006	0.1006

The non-dimensional deflection and stress results at the middle point of single layer [90°] of the laminated composite shell are compared with those of exact solution of Varadan-Bhaskar [38] are presented in Table 5.

Table 5

Non-dimensional deflection $\bar{w}$ and non-dimensional stress $\bar{\sigma}_\xi, \bar{\sigma}_\theta, \bar{\sigma}_z, \bar{\tau}_{\xi z}$ at the middle point of single-layer [90°] of the laminated composite shell $L/R=4; S=R/h; m=1; n=4$

(ξ,θ) (z)	$\bar{w}$ $\left(\frac{\xi}{2},\frac{\theta}{2}\right)$ (0)	$\bar{\sigma}_\theta$ $\left(\frac{\xi}{2},\frac{\theta}{2}\right)$ $(-h/2)$	$\bar{\sigma}_\theta$ $\left(\frac{\xi}{2},\frac{\theta}{2}\right)$ $(+h/2)$	$\bar{\sigma}_\xi$ $\left(\frac{\xi}{2},\frac{\theta}{2}\right)$ $(-h/2)$	$\bar{\sigma}_\xi$ $\left(\frac{\xi}{2},\frac{\theta}{2}\right)$ $(+h/2)$	$\bar{\tau}_{\xi z}$ $\left(\frac{\xi}{2},\frac{\theta}{2}\right)$ $(-h/2)$	$\bar{\tau}_{\xi z}$ $\left(\frac{\xi}{2},\frac{\theta}{2}\right)$ $(+h/2)$	$\bar{\sigma}_z$ $\left(\xi,\frac{\theta}{2}\right)$ (0)
				S=2				
Varadan [38]	7.503	-14.883	5.163	-0.7839	0.1332	-0.1761	0.1430	0.00619
Present	7.367	-13.668	3.643	-0.7939	0.1707	-0.1744	0.1291	0.00405
				S=4				
Varadan [38]	2.783	-6.969	4.859	-0.2295	0.0981	-0.0840	0.0925	0.00619
Present	2.772	-7.076	4.577	-0.2840	0.0892	-0.0831	0.0914	0.00514
				S=10				
Varadan [38]	0.9189	-4.509	4.051	-0.0656	0.0663	-0.0412	0.0436	0.00304
Present	0.9172	-4.529	4.016	-0.0867	0.0553	-0.0411	0.0436	0.00266
				S=50				

Journal Pre-proofs

Varadan [38]	0.5385	-3.979	3.902	-0.0086	0.0845	-0.0383	0.0243	0.00054
Present	0.5384	-3.982	3.897	-0.1220	0.0812	-0.0383	0.0243	0.00044
				S=100				
Varadan [38]	0.5170	-3.876	3.843	0.0288	0.1190	-0.0447	0.0161	0.00026
Present	0.5169	-3.878	3.840	0.0270	0.1173	-0.0447	0.0161	0.00024
				S=500				
Varadan [38]	0.3060	-2.293	2.306	0.1924	0.2459	-0.0611	-0.0249	0.00005
Present	0.3060	-2.293	2.305	0.1922	0.2457	-0.0611	-0.0249	0.00004

From Tables 4 and 5, in comparison with 3D elastic theory [38], we have some discussions as follows

- For [90°/0] shell with large thickness, when S = 4 and 20.6%, the maximum error is 20.6%; for other cases, the maximum error is approximately 5%.

- The relative horizontal normal stresses $\bar{\sigma}_z$ at the middle point of the shell are much smaller than the maximum deflection.

- For thin shell structures, the computed results are almost exact.

- Besides, the appropriateness of calculation results between different theories in the middle of the shell can be explained based on the roots of the characteristic equation (16) and (19). Far away from boundary area, the stress field is determined mainly by the small roots of the characteristic equation (16) and (19), the other large roots only have a big impact in the surrounding areas of jumping stress zone. The values of small roots according to both models $K = 2$ and $K = 3$ are quite close to each other and they are similar to those of Mindlin.

We can ensure that the proposed model and calculation program is verified.

4.2. Effect of boundary conditions

Journal Pre-proofs

In this section, to evaluate effects of boundary conditions, we consider a laminated composite [0/90°] shell made from Graphite-Epoxy (AS/3501) [10] with the thickness h = 0.1 under the distributed load on the inner surface. Boundary conditions include: clamped support - clamped support (C-C), clamped support - simple support (C-S), simple support - simple support (S-S), clamped support - free (C-F), simple support - free (S-F). Non-dimensional deflection and stress are calculated as follows

$$\bar{w} = \frac{10E_1.w}{Q_0 HS^4},\ \left(\bar{\sigma}_\xi, \bar{\sigma}_\theta\right) = \frac{1}{Q_0 S^2}\left(\sigma_\xi, \sigma_\theta\right),\ \bar{\tau}_{\xi z} = \frac{\tau_{\xi z}}{Q_0 S},\ \bar{\sigma}_z = \frac{\sigma_z}{Q_0} \tag{23}$$

Tables 6-8 present non-dimensional deflection $\bar{w}$ and stress $\bar{\sigma}_\xi, \bar{\sigma}_\theta, \bar{\sigma}_z, \bar{\tau}_{\xi z}$ with different relative thickness and boundary conditions for the laminated composite [0/90°] shell.

Table 6

Effect of boundary condition on non-dimensional deflection $\bar{w}$ and stress $\bar{\sigma}_\xi, \bar{\sigma}_\theta, \bar{\sigma}_z, \bar{\tau}_{\xi z}$ of laminated composite [0/90°] shell with parameters L/R=4, S=10

Boundary conditions	$\bar{w}$ $\left(\frac{\xi}{2}, \frac{\theta}{2}\right)$ (0)	$\bar{\sigma}_\xi$ $\left(\frac{\xi}{2}, \frac{\theta}{2}\right)$ $(\pm h/2)$	$\bar{\sigma}_\theta$ $\left(\frac{\xi}{2}, \frac{\theta}{2}\right)$ $(\pm h/2)$	$\bar{\sigma}_z$ $\left(\frac{\xi}{2}, \frac{\theta}{2}\right)$ $(\pm h/4)$	$\bar{\sigma}_\xi$ $\left(\xi, \frac{\theta}{2}\right)$ $(\pm h/2)$	$\bar{\sigma}_\theta$ $\left(\xi, \frac{\theta}{2}\right)$ $(\pm h/2)$	$\bar{\tau}_{\xi z}$ $\left(\xi, \frac{\theta}{2}\right)$ $(\pm h/3)$	$\bar{\sigma}_z$ $\left(\xi, \frac{\theta}{2}\right)$ $(\pm h/4)$
C-C	0.190656	-0.02656 0.01780	-1.7555 -0.0779	-1.3210 3.7998	0.7720 -2.9086	0.3472 -0.1117	-2.6158 3.7355	-1.3210 3.7998
C-S	0.190688	-0.02616 0.02401	-1.7557 -0.0778	0.7441 1.5500	0.0000 0.0000	0.0000 0.0000	-2.6184 2.1405	0.7441 1.5500
S-S	0.190688	-0.02615 0.02397	-1.7557 -0.0778	0.7441 1.5500	0.0000 0.0000	0.0000 0.0000	-2.6184 2.1405	0.7441 1.5500
C-F	0.190688	-0.02616 0.02400	-1.7557 -0.0778	0.5432 0.0973	0.0059 0.0137	-1.7978 -0.0824	-0.3876 -0.0023	0.5432 0.0973
S-F	0.190688	-0.02615 0.02396	-1.7557 -0.0778	0.5432 0.0973	0.0059 0.0137	-1.7978 -0.0823	-0.3876 -0.0023	0.5432 0.0973

Table 7

Journal Pre-proofs

Effect of boundary condition on non-dimensional deflection $\bar{w}$ and stress $\bar{\sigma}_{\xi}, \bar{\sigma}_{\theta}, \bar{\sigma}_{z}, \bar{\tau}_{\xi z}$ of laminated composite [0/90°] shell with parameters *L/R*=4, *S*=50

Boundary conditions	$\bar{w}\left(\frac{\xi}{2},\frac{\theta}{2}\right)$ (0)	$\bar{\sigma}_{\xi}\left(\frac{\xi}{2},\frac{\theta}{2}\right)$ $(\pm h/2)$	$\bar{\sigma}_{\theta}\left(\frac{\xi}{2},\frac{\theta}{2}\right)$ $(\pm h/2)$	$\bar{\sigma}_{z}\left(\frac{\xi}{2},\frac{\theta}{2}\right)$ $(\pm h/4)$	$\bar{\sigma}_{\xi}\left(\xi,\frac{\theta}{2}\right)$ $(\pm h/2)$	$\bar{\sigma}_{\theta}\left(\xi,\frac{\theta}{2}\right)$ $(\pm h/2)$	$\bar{\tau}_{\xi z}\left(\xi,\frac{\theta}{2}\right)$ $(\pm h/3)$	$\bar{\sigma}_{z}\left(\xi,\frac{\theta}{2}\right)$ $(\pm h/4)$
C-C	0.07491	-0.00701 -0.00455	-0.37100 -0.02236	0.52238 0.02846	0.15687 -0.62963	0.07054 -0.02417	2.23979 1.78478	-10.75519 13.88313
C-S	0.07502	-0.00632 0.00628	-0.37122 -0.02216	0.52213 0.02822	0.00000 0.00000	0.00000 0.00000	0.17850 0.84992	0.79540 1.58523
S-S	0.07502	-0.00632 0.00628	-0.37122 -0.02216	0.52213 0.02822	0.00000 0.00000	0.00000 0.00000	0.17850 0.84992	0.79540 1.58523
C-F	0.07502	-0.00517 -0.00521	-0.02382 -0.37486	0.95545 0.46924	0.01008 0.00196	-0.02401 -0.35948	-0.00050 -0.00452	2.11643 0.57941
S-F	0.07502	-0.00632 0.00628	-0.37122 -0.02216	0.52213 0.02822	0.00225 0.01069	-0.38425 -0.02417	-0.00638 -0.00041	0.72798 1.26673

Table 8

Effect of boundary condition on non-dimensional deflection $\bar{w}$ and stress $\bar{\sigma}_{\xi}, \bar{\sigma}_{\theta}, \bar{\sigma}_{z}, \bar{\tau}_{\xi z}$ of laminated composite [0/90°] shell with parameters *L/R*=0.5, *R/h*=10

Boundary conditions	$\bar{w}\left(\frac{\xi}{2},\frac{\theta}{2}\right)$ (0)	$\bar{\sigma}_{\xi}\left(\frac{\xi}{2},\frac{\theta}{2}\right)$ $(\pm h/2)$	$\bar{\sigma}_{\theta}\left(\frac{\xi}{2},\frac{\theta}{2}\right)$ $(\pm h/2)$	$\bar{\sigma}_{z}\left(\frac{\xi}{2},\frac{\theta}{2}\right)$ $(\pm h/4)$	$\bar{\sigma}_{\xi}\left(\xi,\frac{\theta}{2}\right)$ $(\pm h/2)$	$\bar{\sigma}_{\theta}\left(\xi,\frac{\theta}{2}\right)$ $(\pm h/2)$	$\bar{\tau}_{\xi z}\left(\xi,\frac{\theta}{2}\right)$ $(\pm h/3)$	$\bar{\sigma}_{z}\left(\xi,\frac{\theta}{2}\right)$ $(\pm h/4)$
C-C	0.09408	-0.17384 0.86730	-0.88418 -0.00180	0.67648 0.16437	0.69751 -2.45690	0.31363 -0.09432	-2.46575 3.77383	-1.0457 3.4797
C-S	0.12056	-0.20824 1.08111	-1.12769 -0.00141	0.62488 0.12285	0.0000 0.0000	0.0000 0.0000	-2.71752 2.45399	0.7441 1.5500
S-S	0.15686	-0.25336 1.40930	-1.46169 -0.03018	0.55413 0.06589	0.0000 0.0000	0.0000 0.0000	-0.45488 2.47173	0.7441 1.5500
C-F	0.13912	-0.06826 0.22571	-1.28814 -0.04203	0.59083 0.09834	0.00655 0.01810	-2.12321 -0.10488	-2.55159 -0.00148	0.45643 0.06165

Journal Pre-proofs

S-F	0.13912	-0.06836	-1.28814	0.59083	0.00655	-2.12321	-2.55159	0.45643
		0.22571	-0.04203	0.09834	0.01810	-0.10488	-0.00148	0.06165

Analyzing the obtained results, we have some comments as follows

- For shell structures, which have the length is larger than the average value, at the area far from the boundary zone, boundary conditions have a light effect on the deflection and stress.

- The area near boundary zone, the maximum stress of the shell structure depends on the type of boundary conditions. There is a big stress jumping zone for the case of C-C type.

- The shorter the length of the shell structure is, the more boundary conditions affect to the deflection and stress at the center of the structure.

Now, the following figures present the non-dimensional stress distribution by the thickness of the composite isotropic shell (R/h=10, L/R= 4, h=0.1) at the surrounding C-C boundary condition. The structure is impacted by the distributed load on the inner surface.

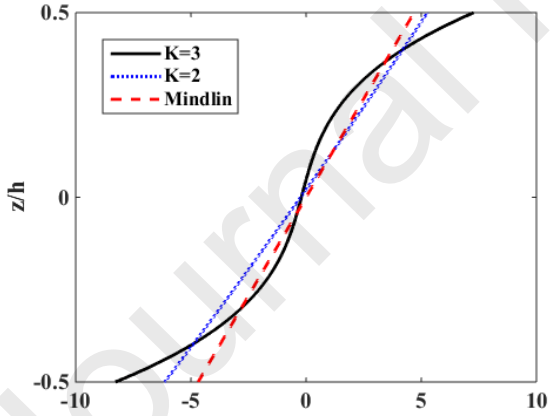

a) $\bar{\sigma}_{\xi}$ stress at the boundary position

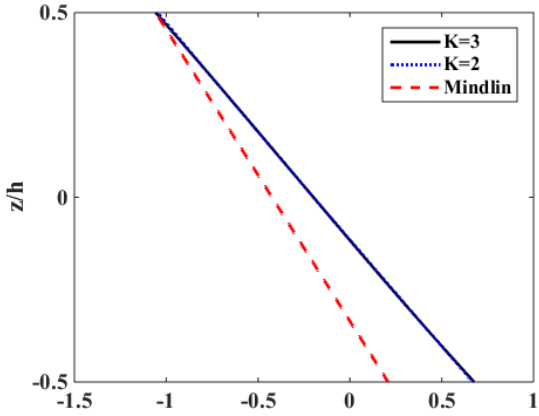

b) $\bar{\sigma}_{\xi}$ stress is at 5h distance from the boundary

Journal Pre-proofs

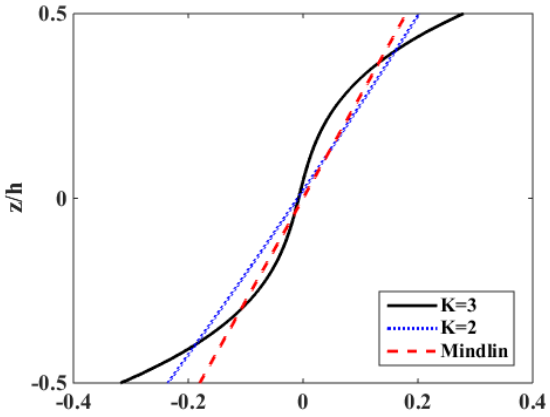

c) $\bar{\sigma}_\theta$ stress at the boundary position

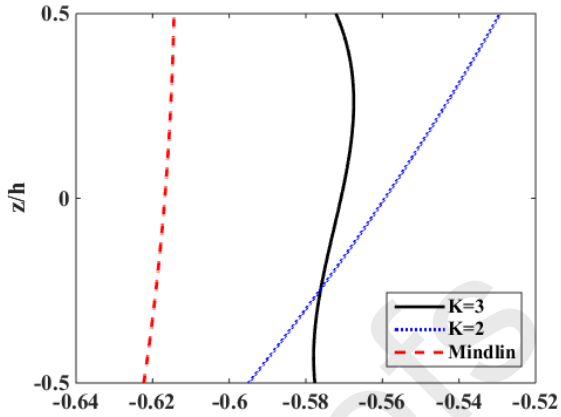

d) $\bar{\sigma}_\theta$ stress is at 5h distance from the boundary

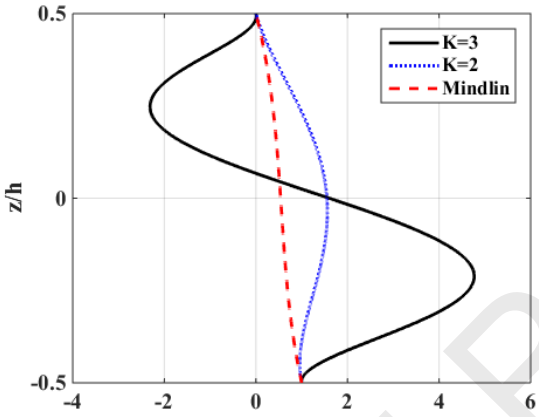

e) $\bar{\sigma}_z$ stress at the boundary position

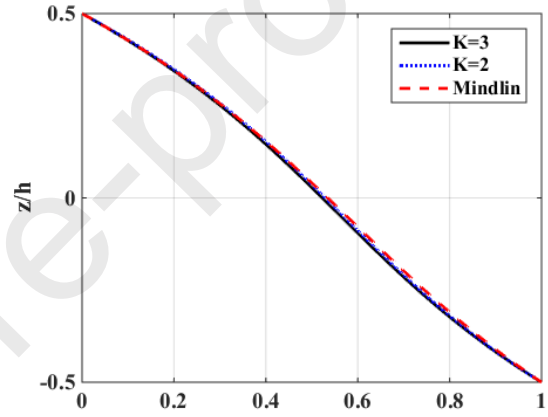

f) $\bar{\sigma}_z$ stress is at 5h distance from the boundary

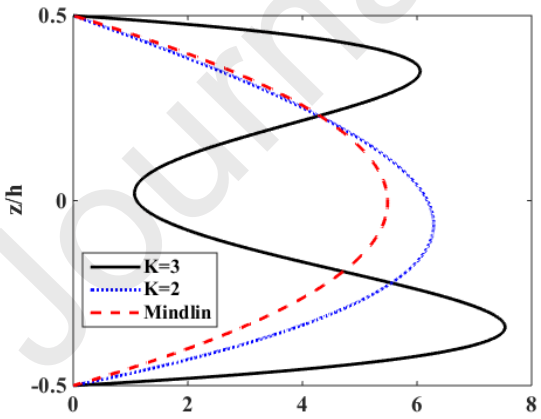

) $\bar{\tau}_{\xi z}$ stress at the boundary position

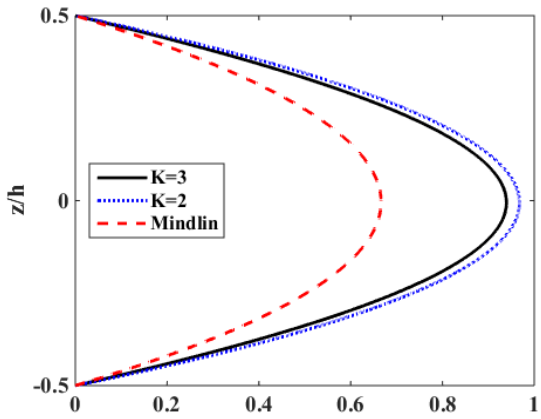

h) $\bar{\tau}_{\xi z}$ stress is at 5h distance from the boundary

Figure 3. Non-dimensional stress distribution by the thickness of composite isotropic shell; R/h=10, L/R= 4, h=0.1

Journal Pre-proofs

From the computed results of the stress distribution at a distance h from the boundary, we can see that the proposed theory and calculation program meet a very good agreement. This can be explained as follows: the stress at the far points from the boundary is determined by the small roots $\pm p_1 \pm iq_1$ of characteristic equations (16) and (19). Also, these roots are quite similar to one another and to those of Mindlin theory (see Tables 1-3). In the boundary zone, the stress field is strongly influenced by the large roots; the size of the affected area of this stress jumping zone is approximately equal to the shell thickness. The above analysis shows that for thin composite cylindrical shells, using higher-order shear deformation shell theory give higher results at the surrounding boundary condition in comparison with the classical theory.

4.3. Effect of the relative length L/R

Next, let us consider a C-C laminated composite [0/90°] shell made from Graphite-Epoxy (AS/3501) [10] with the thickness h = 0.1, and the relative length L/R=4; the shell is under the distributed load on the inner surface. Non-dimensional deflection $\bar{w}$ and stresses $\bar{\sigma}_\xi, \bar{\sigma}_\theta, \bar{\sigma}_z, \bar{\tau}_{\xi z}$ are listed in Table 9.

Table 9

Effect of the relative length L/R on non-dimensional deflection $\bar{w}$ and stresses $\bar{\sigma}_\xi, \bar{\sigma}_\theta, \bar{\sigma}_z, \bar{\tau}_{\xi z}$ of C-C laminated composite [0/90°] shell; S=10

L/R	$\bar{w}$ $\left(\frac{\xi}{2},\frac{\theta}{2}\right)$ (0)	$\bar{\sigma}_\xi$ $\left(\frac{\xi}{2},\frac{\theta}{2}\right)$ $(\pm h/2)$	$\bar{\sigma}_\theta$ $\left(\frac{\xi}{2},\frac{\theta}{2}\right)$ $(\pm h/2)$	$\bar{\sigma}_z$ $\left(\frac{\xi}{2},\frac{\theta}{2}\right)$ $(\pm h/4)$	$\bar{\sigma}_\xi$ $\left(\xi,\frac{\theta}{2}\right)$ $(\pm h/2)$	$\bar{\sigma}_\theta$ $\left(\xi,\frac{\theta}{2}\right)$ $(\pm h/2)$	$\bar{\tau}_{\xi z}$ $\left(\xi,\frac{\theta}{2}\right)$ $(\pm h/3)$	$\bar{\sigma}_z$ $\left(\xi,\frac{\theta}{2}\right)$ $(\pm h/4)$
0.5	0.09408	-0.17384	-0.88418	0.67648	0.69751	0.31363	2.46575	-1.0457
		0.86730	-0.00180	0.16437	-2.45690	-0.09432	3.77383	3.47971
1	0.195613	-0.09866	-1.80544	0.48135	0.78419	0.35260	2.65129	-1.35804
		0.49533	-0.07171	0.01118	-2.93721	-0.11276	3.75136	3.83021

2	0.191839	-0.02264 0.00083	-1.76608 -0.07893	0.48962 0.01903	0.77257 -2.90430	0.34738 -0.11150	2.61771 3.73391	-1.32292 3.79870
4	0.190656	-0.02656 0.01780	-1.7555 -0.0779	0.49186 0.02076	0.7720 -2.9086	0.34720 -0.11167	2.61578 3.73551	-1.32101 3.79982
10	0.190642	-0.02672 0.01505	-1.75539 -0.07793	0.49189 0.02078	0.77165 -2.91124	0.34697 -0.11177	2.61465 3.73652	-1.31986 3.80050

Table 9 shows that for the short shell structure ($L/R \le 2$), the relative has a small effect on the strain and stress fields of the structure. When the relative length $L/R \ge 4$, deflection and stress in similar locations do not have an obvious difference. Besides, from Tables 6 and 8 we understand that when $L/R \le 1$, boundary conditions affect strongly to the deflection and stress; when $L/R \ge 4$, boundary condition does not affect much to the maximum stress.

4.4. Effect of relative thickness S=R/h

Table 10 presents the non-dimensional deflection $\bar{w}$ and stress $\bar{\sigma}_\xi, \bar{\sigma}_\theta, \bar{\sigma}_z, \bar{\tau}_{\xi z}$ of C-C laminated composite [0/90°] shell with different relative thickness *S*.

Table 10

Effect of relative thickness *S* on non-dimensional deflection $\bar{w}$ and stresses $\bar{\sigma}_\xi, \bar{\sigma}_\theta, \bar{\sigma}_z, \bar{\tau}_{\xi z}$ of C-C laminated composite [0/90°] shell; *L/R*=4, *h*=0.1

S	$\bar{w}$ $\left(\frac{\xi}{2},\frac{\theta}{2}\right)$ (0)	$\bar{\sigma}_\xi$ $\left(\frac{\xi}{2},\frac{\theta}{2}\right)$ $(\pm h/2)$	$\bar{\sigma}_\theta$ $\left(\frac{\xi}{2},\frac{\theta}{2}\right)$ $(\pm h/2)$	$\bar{\sigma}_z$ $\left(\frac{\xi}{2},\frac{\theta}{2}\right)$ $(\pm h/4)$	$\bar{\sigma}_\xi$ $\left(\xi,\frac{\theta}{2}\right)$ $(\pm h/2)$	$\bar{\sigma}_\theta$ $\left(\xi,\frac{\theta}{2}\right)$ $(\pm h/2)$	$\bar{\tau}_{\xi z}$ $\left(\xi,\frac{\theta}{2}\right)$ $(\pm h/3)$	$\bar{\sigma}_z$ $\left(\xi,\frac{\theta}{2}\right)$ $(\pm h/4)$
10	0.190656	-0.02656 0.01780	-1.7555 -0.0779	0.49186 0.02076	0.7720 -2.9086	0.34720 -0.11167	2.61578 3.73551	-1.32101 3.79982
20	0.0471	-0.01577 -0.00333	-0.9094 -0.0490	0.5105 0.0254	0.3987 -1.5234	0.1793 -0.0585	-2.4826 2.7022	-3.6805 6.3566

Journal Pre-proofs

30	0.02087	-0.01115 0.00513	-0.6130 -0.0352	0.5170 0.0271	0.2652 -1.0341	0.1193 -0.0397	-2.3768 2.2443	-6.0489 8.8834
40	0.01172	-0.00861 -0.00500	-0.4623 -0.0274	0.5204 0.0279	0.1975 -0.7828	0.0888 -0.0300	-2.2992 1.9711	-8.4071 11.3903
50	0.00750	-0.00701 -0.00455	-0.3710 -0.0234	0.5224 0.0285	0.1569 -0.6296	0.0705 -0.0241	-2.2398 1.7848	-10.7555 13.8831

The stress distribution by the thickness at several points of the [0/90°/0] shell structure with different relative thicknesses is shown in the following figure.

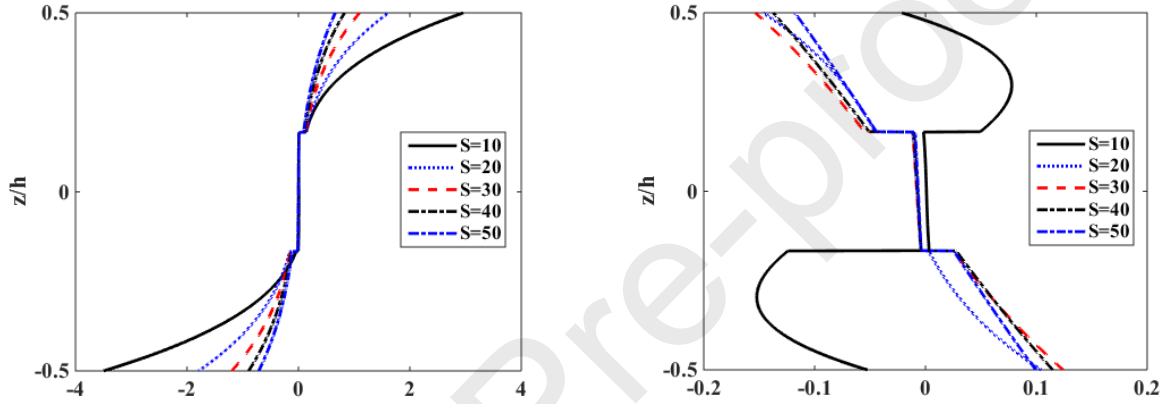

a1) $\bar{\sigma}_{\xi}$ stress at the boundary position

a2) $\bar{\sigma}_{\xi}$ stress is at 5*h* distance from the boundary

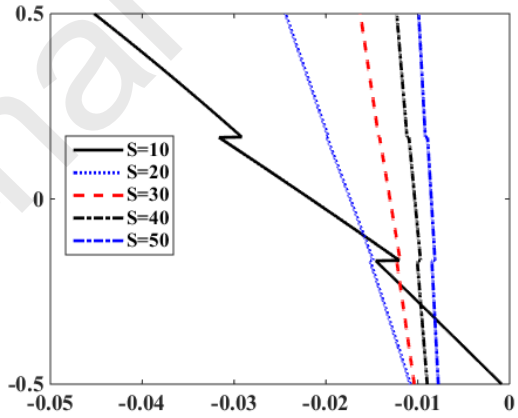

a3) $\bar{\sigma}_{\xi}$ stress at $\xi = \xi_0 / 2$

Journal Pre-proofs

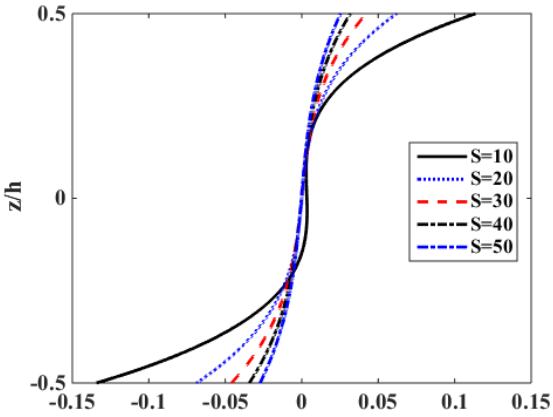

b1) $\bar{\sigma}_\theta$ stress at the boundary position

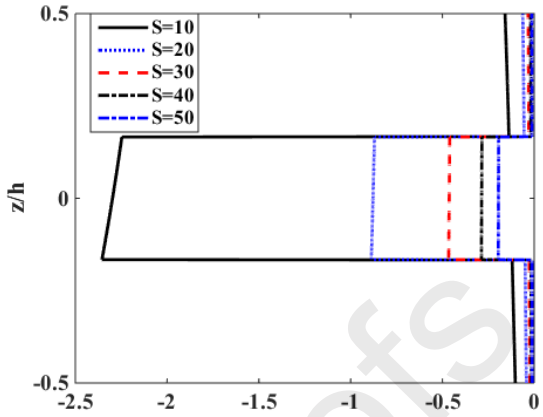

b2) $\bar{\sigma}_\theta$ stress is at 5*h* distance from the boundary

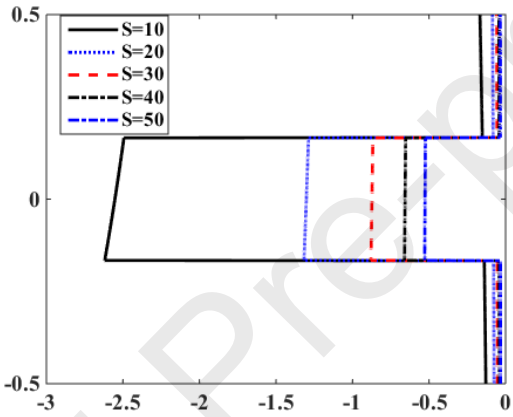

b3) $\bar{\sigma}_\theta$ stress at $\xi = \xi_0 / 2$

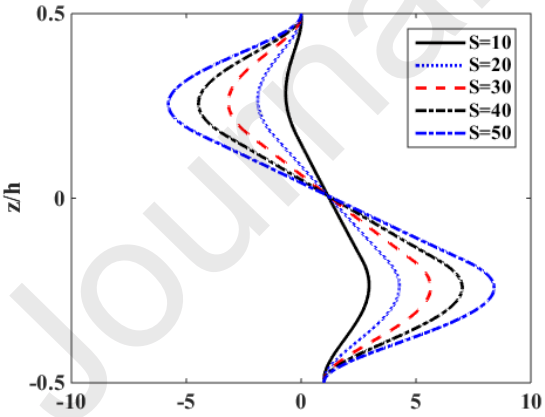

c1) $\bar{\sigma}_z$ stress at the boundary position

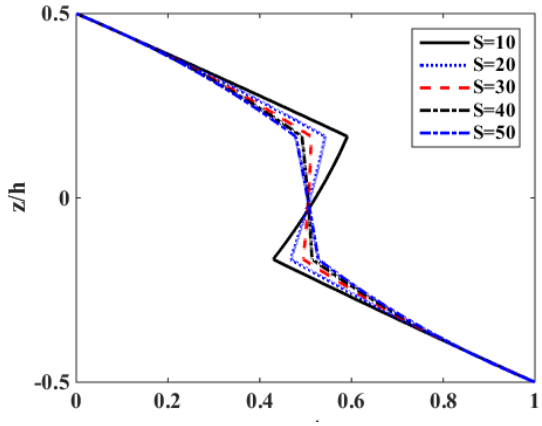

c2) $\bar{\sigma}_z$ stress is at 5*h* distance from the boundary

Journal Pre-proofs

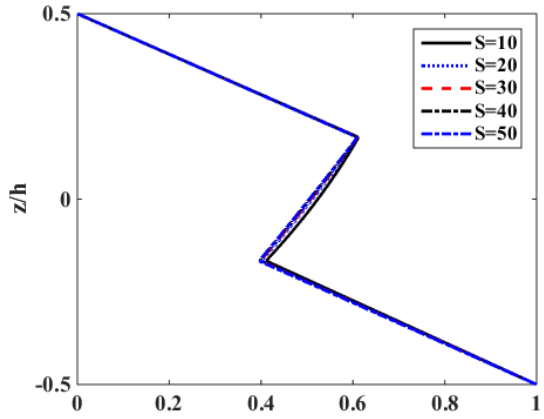

c3) $\bar{\sigma}_z$ stress at $\xi = \xi_0 / 2$

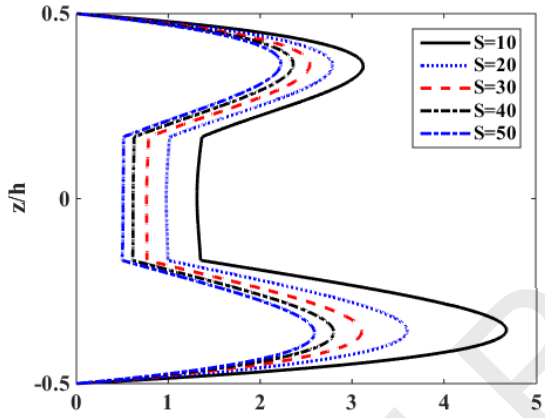

d1) $\bar{\tau}_{\xi z}$ stress at the boundary position

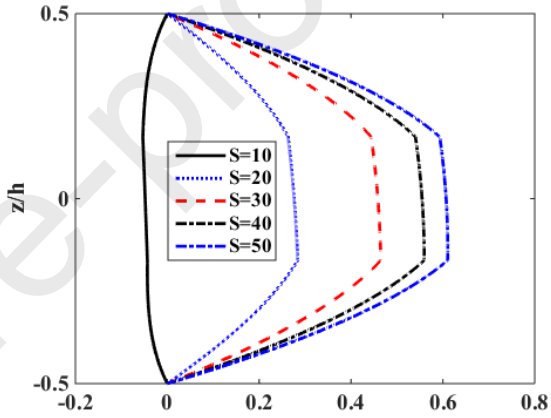

d2) $\bar{\tau}_{\xi z}$ stress is at 5*h* distance from the boundary

Figure 5. The stress distribution of the [0/90°/0] shell structure; *L/R*=4; *h*=0.1; material type Gr.Ep_AS

From the above figure, we have some discussions as follows

- The thickness of shell effects strongly on the deflection and stress of shell structure.

- Boundary phenomenon occurs for both thin and thick shell, and it is approximately 1.4 time of maximum stress.

- The thicker the thickness is, the larger the jumping zone phenomenon gets.

5. Conclusion

Based on the proposed theory and computed results presented in this work, we have some highlight conclusions as follows

Journal Pre-proofs

- The equations for analyzing the cylindrical shell according to the high-order shear deformation theory of quasi-3D type are established; in which the displacement field is analyzed into polynomials according to the shell thickness. The mathematical model and computed results are compared with those according to 3D elastic theory, thereby confirming the reliability of the results obtained in this work. The models presented in this paper take into account the effects of the horizontal normal stress (which are neglected in terms of first-order shear deformation theory and high-order deformation theory), thus, we can expand the area of application for these models.

- The roots of the characteristic equation are divided into a small root group and a large root group. The small one characterizes the stress field far from the region of metamorphic stress field (the boundary area, structural jumping, force jumping and so on), while the other one has a great influence on the stress field of the metamorphic stress field

- Effects of boundary conditions, lamination sequence, relative thickness (R/h), and relative length of the shell structure (L/R) on deflection and stress are investigated. The parameter studies show that the thickness of shell as well as boundary conditions and lamination sequence effect strongly on the deflection and stress of shell structure.

- In the boundary zone, the stress field is influenced by the marginal effects, corresponding to the large roots of the characteristic equation, so when determining the stress field in the boundary region, it is necessary to use the higher-order shear deformation shell theory.

- In the region far from boundary area, the obtained results based on 3D elastic theory, Mindlin's theory and this work are approximately equal.

References

Journal Pre-proofs

[1] Aeromagazine. Boing 787 from the ground up. The Boeing Company 2006, 17-23 Print.

[2] Timoshenko S, Woinowsky-Krieger S. Theory of plates and shells. McGrawHill 1959.

[3] Flügge W. Stresses in shells. Springer-Verlag1960.

[4] Gol'Denveizer AL. Theory of elastic thin shells. Solid and Structural Mechanics- Pergamon Press 1961.

[5] Novozhilov VV. Thin shell theory. P. Noordhof 1964.

[6] Leissa AW. Vibration of shells. NASA-SP-288 1973.

[7] Reissner E. On transverse bending of plates, including the effect of transverse shear deformation. International Journal of Solids and Structures 1975; 11 (5); pp. 569-573.

[8] Kraus H. Thin elastic shells. John Wiley & Sons 1976.

[9] Gould PL. Analysis of plates and shells. Prentice-Hall 1999.

[10] Reddy JN. Mechanics of laminated composite plate and shell theory and analysis – 2nd edition. CRC Press 2004.

[11] Asadi E, Wang W, Qatu MS. Static and vibration analyses of thick deep laminated cylindrical shells using 3D and various shear deformation theories. Composite Structures 2012; 94 (2); pp. 494-500.

[12] Liu B, Xing YF, Qatu MS, Ferreira AJM. Exact characteristic equations for free vibrations of thin orthotropic circular cylindrical shells. Composite Structures 2012; 94 (2); pp. 484-493.

[13] Mantari JL, Oktem AS, Guedes Soares C. A new higher order shear deformation theory for sandwich and composite laminated plates. Composites Part B 2012; 43 (3); pp. 1489-1499.

[14] Kant T, Swaminathan K. Analytical solutions for the static analysis of laminated composite and sandwich plates based on a higher order refined theory. Composite Structures 2002; 56 (4); pp. 329-344.

[15]. Tran TT, Nam HN, Thom DV, Phung VM, Duc ND. Bending and thermal buckling of unsymmetric functionally graded sandwich beams in high-temperature environment based on a new third-order shear deformation theory. Journal of Sandwich Structures & Materials 2019; 0(0); pp. 1–25.

[16]. Nam HN, Tran CT, Luat DT, Van DP, Thom DV, Phung VM. research on the buckling behavior of functionally graded plates with stiffeners based on the third-order shear deformation theory. Materials 2019; 12; 0; 30 pages.

[17]. Nam HN, Tan YN, Ke TV, Thanh TT, Truong TN, Van DP, Thom DV. A finite element model for dynamic analysis of triple-layer composite plates with layers connected by shear connectors subjected to moving load. Materials 2019; 12; 598; 19 pages.

[18]. Nam HN, Hong TT, Pham VV, Nguyen DQ, Thom DV. A refined simple first-order shear deformation theory for static bending and free vibration analysis of advanced composite plates. Materials 2019; 12; 2385; 25 pages.

[19]. Nam HN, Canh TN, Thanh TT, Tran VK, Van DP, Thom DV. Finite element modelling of a composite shell with shear connectors. Symmetry 2019; 11; 527; 22 pages.

Journal Pre-proofs

[20]. Nam HN, Tran TH, Pham VV, Thom DV. An efficient beam element based on quasi-3d theory for static bending analysis of functionally graded beams. Materials 2019; 12; 2198; 22 pages.

[21]. Vu HN, Duc HD, Nguyen MK, Thom DV, Hong TT. Phase-field buckling analysis of cracked stiffened functionally graded plates. Composite Structures 2019; 217; pp. 50-59.

[22]. Tien DP, Quoc HP, Van DP, Hoang NN, Thom DV. Free vibration analysis of functionally graded shells using an edge-based smoothed finite element method. Symmetry 2019; 11; 68; 19 pages.

[23] Lei J, Yongjian L, Amir F. Stress concentration factors in concrete-filled square hollow section joints with perfobond ribs. Engineering Structures 2019; 181; pp. 165-180.

[24] Go Y, Miho O, Keita K, Jun W, Haruki O, T, Tomonaga O. Considering the stress concentration of fiber surfaces in the prediction of the tensile strength of unidirectional carbon fiber-reinforced plastic composites. Composites Part A 2019; 121; pp. 499-509.

[25] Özaslan E, Bülent A, Mehmet AG. Experimental and numerical investigation of stress concentration and strength prediction of carbon/epoxy composites. Procedia Structural Integrity 2018; 13; pp. 535-541.

[26] Ahmed T, Choudhry RS, Shah AUR, Hasan AS. A study on finite element of pre damaged stress concentration factor for a composite laminate member with central circular. Journal of Mechanical Science and Technology 2018; 32 (8); pp. 3653–3658.

[27]. Fukada Y. Stress redistribution as an effect of non-uniform in-plane laminate stresses in laminate composite plates. Composite Structures 2017; 159; pp. 505–516.

[28]. Arshid E, Khorshidvand AR. Free vibration analysis of saturated porous FG circular plates integrated with piezoelectric actuators via differential quadrature method. Thin-Walled Structures 2018; 125; pp. 220–233.

[29]. Li DH. Extended layerwise method of laminated composite shells. Composite Structures 2016; 136; pp. 313–344.

[30]. Akgöz B, Civalek O. Nonlinear vibration analysis of laminated plates resting on nonlinear two-parameters elastic foundations. Steel Compos Struct 2011; 11; pp. 403–421.

[31]. Civalek O, Acar MH. Discrete singular convolution method for the analysis of Mindlin plates on elastic foundations. Int J Press Vessel Pip 2007; 84 (9); pp. 527–535.

[32]. Civalek O. Linear vibration analysis of isotropic conical shells by discrete singular convolution (DSC). Structural Engineering and Mechanics 2007; 25(1); pp.127–130.

[33]. Civalek O. Vibration analysis of conical panels using the method of discrete singular convolution.

Journal Pre-proofs

Communications in Numerical Methods in Engineering 2008; 24; pp.169–181.

[34]. Patnia M, Mineraa S, Groha RMJ, Pirreraa A,Weaver PM. On the accuracy of localised 3D stress fields in tow-steered laminated composite structures. Composite Structures 2019; 225; 111034.

[35] Firsanov VV, Doan TN. Investigation of the statics and free vibrations of cylindrical shells on the basis of a nonclassical theory. Composites Mechanics Computations Applications: An International Journal 2015; 6 (2); pp. 135-166.

[36] Vasiliev VV and Lurie SA. To a problem of improvement of the theory of shallow shells. Izv. RAN, Mekh-Tverd-Tela 1990; 6; pp. 139–146.

[37] Mindlin RD. An introduction to the mathematical theory of vibrations of elastic plates. World Scientific Publishing 2006.

[38] Varadan TK and Bhaskar K. Bending of laminated orthotropic cylindrical shells an elasticity approach. Composite Structures1991; 17 (2); pp. 141-156.

Appendix

The value of each element in the matrix $\left[C^{(k)}\right]$

$$C_{11}^{(k)}=\frac{E_1^{(k)}\left(1-\mu_{23}^{(k)}\mu_{32}^{(k)}\right)}{\mu^{(k)}},\quad C_{12}^{(k)}=\frac{E_1^{(k)}\left(\mu_{21}^{(k)}+\mu_{31}^{(k)}\mu_{23}^{(k)}\right)}{\mu^{(k)}},$$

$$C_{13}^{(k)}=\frac{E_1^{(k)}\left(\mu_{31}^{(k)}+\mu_{21}^{(k)}\mu_{32}^{(k)}\right)}{\mu^{(k)}},\quad C_{22}^{(k)}=\frac{E_2^{(k)}\left(1-\mu_{13}^{(k)}\mu_{31}^{(k)}\right)}{\mu^{(k)}},$$

$$C_{23}^{(k)}=\frac{E_2^{(k)}\left(\mu_{32}^{(k)}+\mu_{12}^{(k)}\mu_{31}^{(k)}\right)}{\mu^{(k)}},\quad C_{33}^{(k)}=\frac{E_3^{(k)}\left(1-\mu_{12}^{(k)}\mu_{21}^{(k)}\right)}{\mu^{(k)}},$$

$$C_{44}^{(k)}=G_{12}^{(k)},\quad C_{55}^{(k)}=G_{13}^{(k)},\quad C_{66}^{(k)}=G_{23}^{(k)},$$

$$\mu^{(k)}=\left(1-\mu_{12}^{(k)}\mu_{21}^{(k)}-\mu_{23}^{(k)}\mu_{32}^{(k)}-\mu_{13}^{(k)}\mu_{31}^{(k)}-2\mu_{13}^{(k)}\mu_{32}^{(k)}\mu_{21}^{(k)}\right).$$

where E is Young's modulus, G is shear modulus, and μ is Poisson's ratio of layer; they have relations as follows

$$\frac{\mu_{12}^{(k)}}{E_1^{(k)}}=\frac{\mu_{21}^{(k)}}{E_2^{(k)}},\quad \frac{\mu_{13}^{(k)}}{E_1^{(k)}}=\frac{\mu_{31}^{(k)}}{E_3^{(k)}},\quad \frac{\mu_{23}^{(k)}}{E_2^{(k)}}=\frac{\mu_{32}^{(k)}}{E_3^{(k)}}.$$

Journal Pre-proofs

The value of each element in the matrix $\left[Q^{(k)}\right]$

$$Q_{11}^{(k)} = C_{11}^{(k)}c^4 + 2\left(C_{12}^{(k)} + 2C_{44}^{(k)}\right)s^2c^2 + C_{22}^{(k)}s^4,\ Q_{12}^{(k)} = C_{12}^{(k)}\left(c^4 + s^4\right) + \left(C_{11}^{(k)} + C_{22}^{(k)} - 4C_{44}^{(k)}\right)s^2c^2,$$

$$Q_{13}^{(k)} = C_{13}^{(k)}c^2 + C_{23}^{(k)}s^2,\ C_{14}^{(k)} = \left(C_{11}^{(k)} - C_{12}^{(k)} - 2C_{44}^{(k)}\right)sc^3 + \left(C_{12}^{(k)} - C_{22}^{(k)} + 2C_{44}^{(k)}\right)cs^3,$$

$$Q_{22}^{(k)} = C_{11}^{(k)}s^4 + C_{22}^{(k)}c^4 + 2\left(C_{12}^{(k)} + 2C_{44}^{(k)}\right)s^2c^2,\ Q_{23}^{(k)} = C_{13}^{(k)}s^2 + C_{23}^{(k)}c^2,$$

$$Q_{24}^{(k)} = \left(C_{11}^{(k)} - C_{12}^{(k)} - 2C_{44}^{(k)}\right)cs^3 + \left(C_{12}^{(k)} - C_{22}^{(k)} + 2C_{44}^{(k)}\right)sc^3,\ Q_{33}^{(k)} = C_{33}^{(k)},\ Q_{34}^{(k)} = \left(C_{13}^{(k)} - C_{23}^{(k)}\right)sc,$$

$$Q_{44}^{(k)} = \left(C_{11}^{(k)} - 2C_{12}^{(k)} + C_{22}^{(k)} - 2C_{44}^{(k)}\right)c^2s^2 + C_{44}^{(k)}\left(c^4 + s^4\right),\ Q_{55}^{(k)} = C_{55}^{(k)}c^2 + C_{66}^{(k)}s^2,$$

$$Q_{56}^{(k)} = \left(C_{66}^{(k)} - C_{55}^{(k)}\right)cs,\ Q_{66}^{(k)} = C_{55}^{(k)}s^2 + C_{66}^{(k)}c^2,$$

Also we have equations $Q_{ij}^{(k)} = Q_{ji}^{(k)}$ for $i, j = 1...6$ and $c = \cos\beta$, $s = \sin\beta$.

Journal Pre-proofs